NONLINEAR RHEOLGY OF ENTANGLED POLYMERS: IMPLICATIONS OF SHEAR BANDING AND INTERFACIAL SLIP

A Dissertation

Presented to the Faculty of the Graduate School

of Cornell University

In Partial Fulfillment of the Requirements for the Degree of

Doctor of Philosophy

by

Keesha Hayes

August 2009

NONLINEAR RHEOLGY OF ENTANGLED POLYMERS: IMPLICATIONS OF SHEAR BANDING AND INTERFACIAL SLIP

Keesha Hayes, Ph.D.

Cornell University 2009

The Doi-Edwards (D-E) molecular, viscoelastic theory for entangled polymers is used as the framework for an experimental study of flow anomalies in well-characterized polymer solutions and melts, spanning a wide range of entanglement densities. Results of linear viscoelastic and nonlinear rheology experiments – steady and step shear - were compared to existing theory. Unlike weakly and moderately entangled polymers ($N/N_e \leq 11$), the step-shear damping function, $h(\gamma) = G(t, \gamma)/ G(t, \gamma \rightarrow 0)$, for polymers with high entanglement densities is more strain softening than the Doi-Edwards prediction, $h_{D\text{-}E}(\gamma)$.

Two likely causes of this deviation, commonly called type C Damping, are interfacial slip and shear banding. To isolate the mechanism(s) responsible for the discrepancy, we combine macroscopic techniques (rheometry) with direct visualization (confocal microscopy and particle image velocimetry) during steady shear flow. In the latter case, this high resolution measurement technique allows us to construct the velocity profile in narrow-gap, planar-Couette shear flow. Importantly, even for shear rates well into the non-Newtonian shear-rate regime, where the unmodified D-E theory predicts shear banding, all the shear profiles are found to be linear. There is strong evidence of interfacial slip, which can be characterized and compared to slip theories for entangled polymers.

To remove/ weaken the role of slip, the original confocal set-up was modified to allow both a transient shear and large-gap study. These results were compared with qualitative expectations from transient constitutive curves: $\sigma(\dot{\gamma})$ *vs.* $\dot{\gamma}$, measured at similar times in mechanical rheometry experiments. During start-up of steady shear flow, rheometry measurements show a maximum in $\sigma(\dot{\gamma})$ *vs.* $\dot{\gamma}$ at times prior to steady state. To determine whether this transient, non-monotonic stress growth leads to transient shear banding, we characterized the velocity profile as a function of time. Surprisingly, these measurements again yield decidedly linear profiles that vary little with time, indicating that there is some feature of the shear flow that stabilizes it against banding.

Finally, step shear experiments with entangled star-branched polymer solutions reveal that the damping function is universal but different from $h_{D\text{-}E}(\gamma)$. And, linear and nonlinear rheology of unentangled stars indicates that their flow behavior follows Rouse model predictions.

BIOGRAPHICAL SKETCH

Keesha Alicia Hayes was born in San Fernando, Trinidad & Tobago on October 2nd, 1980. She grew up with her parents and two younger brothers in Trinidad, and then moved to the United States in 2000 to pursue her undergraduate degree. In August 2000, she enrolled at Howard University in Washington, D.C. During her time as an undergraduate she did a research internship (REU) at Cornell University and two company internships: at SC Johnson & Son, Inc. and Corning, Inc. In May, 2004 she graduated Summa cum Laude with a B.S. in Chemical Engineering from Howard University. In August of that same year, she enrolled in the chemical engineering department at Cornell University.

to my parents – Randolph and Aulda Hayes and my two brothers – Kevon and Keon

for their unconditional love and unwavering support

ACKNOWLEDGMENTS

I would like to thank my advisor Dr. Lynden Archer for his invaluable guidance on this project. His excitement and enthusiasm about Polymer Physics has been both inspirational and contagious. I am very grateful for his hands-on training and dedicated teaching, which provided me with the tools needed to make progress towards my research goals.

I would also like to thank the other student members of the Archer group for creating a cooperative work environment and for the discussions, which often sparked an idea or led to a problem solution. A special thank you to the Itai Cohen research group in the Department of Physic. Dr. Cohen and his students graciously gave me unlimited access to their lab facilities, office space and expertise. I am also thankful to my committee members – Dr. Claude Cohen and Dr. Dotsevi Sogah – for useful discussions.

Finally, I'd like to thank my dear friends and all the people – too many to list – who helped to make my experience at Cornell so wonderful.

TABLE OF CONTENTS

LIST OF FIGURES

LIST OF TABLES

CHAPTER 1

Introduction

Successful prediction of flow behavior in entangled polymers is important in a multitude of commercial processes used for molding, extruding, and spinning plastic components. The Doi-Edwards (D-E) constitutive theory provides the most successful molecular framework for understanding polymer flow properties. The D-E Theory is a molecular viscoelastic theory for molten, high molecular weight polymers that uses the reptation concept [1]. This concept says that, because of the presence of neighboring molecules, there are many places along a polymer chain where lateral motion is restricted, forcing the molecule to reptate along a "tube".

Doi and Edwards examined the ways the chain can respond to a change in tube configuration caused by deformation and developed a constitutive model to describe this. The imposition of sudden shear causes affine deformation of the primitive chain and the stresses built up in the polymer relax by two mechanisms. On short time scales, of order the Rouse relaxation time, τ_{Rouse}, the chain retracts down the deformed tube to recover its equilibrium contour length. The remaining stresses, due to anisotropic segmental orientation, relax by reptation until the primitive chain finally escapes the tube [2].

The Doi-Edwards Tube Theory, which works well in predicting the step-shear flow in most entangled polymers, predicts a steady-state stress maximum (of order the plateau modulus, G_N) at a shear rate of order the chain disengagement time, τ_d^{-1}. The stress then falls continuously to zero with increasing shear rate – a scenario that is physically unrealistic. The controversial issue of whether or not highly entangled polymers exhibit a monotonic constitutive relation in steady shear flow has been extensively investigated both theoretically and experimentally [3 - 6].

One driving force for interest in this area is that predicting the constitutive relation between an applied flow field and the corresponding stress is crucial to industrial processes like extrusion. Doi and Edwards were the first to relate the spurt instability in

capillary flow to this theoretical stress maximum [7]. More recently than this, the multi-valued, shear stress instability has been linked to the shear banded flow predicted in numerical simulations [8], detected in flow birefringence [9] and in NMR velocity imaging [10] experiments.

Shear banding is when adjacent fluid layers have uniform but different shear rates. At the band interface, the shear stress and the normal stress component perpendicular to the interface are both continuous [11]. The exact mechanism that causes this phenomenon is not fully understood. However, it is largely believed to be due to the kind of constitutive instability predicted by Doi-Edwards. If the applied shear rate is in the region after the stress maximum, this yields mechanically unstable flow [12] and the fluid separates into shear rate bands. Other proposed mechanisms for shear banding in viscoelastic fluids are shear induced concentration fluctuations [13], and secondary flow in geometries like cone & plate [14].

Shear banding has not yet been irrefutably observed in polymers. So, attempts have been made to "fix" the theory, so that it better describes polymers in steady shear [15], while still maintaining its accuracy in step shear predictions. Most of these theories eliminate the stress maximum by incorporating the effects of convective constraint release (CCR) – the polymer chain convected through its confining tube in fast flows and/or chain stretching – flow induced changes in tube contour length.

While detection of shear banding in entangled polymers is somewhat elusive, there are several experimental examples of shear banding in aqueous surfactant systems like cetylpyridinium chloride and sodium salicylate (CPyCL/NaSl) in water. In flow birefringence with a surfactant solution in co-cylinder Couette geometry, Beret et al [16] detected a bright band near the inner cylinder. And, steady shear rheometry data from Rehage & Hoffman for the aforementioned CPyCL/NaSl system [17] was in excellent agreement with model predictions [18] for micelles sheared in the stress plateau region.

Shear banding is almost always detected in high-shear-rate flow of wormlike micellar systems. And, the D-E prediction for the steady-shear stress response in polymers is qualitatively similar to the constitutive prediction for micelles [18]. But, our ability to decisively "see" shear banding (if it is present) in entangled polymers might always be hindered by factors like unreliable high-shear-rate behavior (edge fracture) and polymer polydispersity. The question of whether entangled polymers can shear band, even though all recent theories have assumed that they do not, is an important one. A different approach, and the one employed in this work, is the design and execution of novel steady shear experiments for testing the original D-E prediction.

An important challenge in doing high-shear-rate experiments with entangled polymers is the flow instability called interfacial slip. In fact, slip at the fluid-solid interface also affects large-strain, step-shear experiments, leading to discrepancies between experiment and the D-E prediction [19]. Unlike steady shearing of polymers, step shear is not widespread in "real-world" polymer processing. However, this instantaneous deformation is the most dramatic way that one can perturb the polymer chain; so, analyzing the polymer's response is a useful tool for gleaning information about any flow anomalies that occur after deformation. Both shear banding and slip can affect experimental results and differentiating between the two in not trivial.

In the hydrodynamic no-slip condition, the tangential velocity of a liquid in contact with a solid substrate is the same as the velocity of the substrate. This hypothesis, which has no microscopic justification, assumes that fluid molecules next to a surface do not slide (slip) over the surface. Instead, they adhere to it due to attractive forces between fluid and surface molecules at the interface. Experiments show that the no-slip condition is violated for simple liquids near chemically modified surfaces or surfaces that are smooth on the order of the molecular size of the fluid [20-21]. But, most slip evidence comes via studies with complex fluids like polymer melts and surfactants [22]. In complex

slip occurs by three main mechanisms:

I. Cohesive Slip – interrupted momentum transport between bulk fluid and surface-adsorbed fluid.

II. Lubrication slip – one fluid lubricating the flow of another e.g. a near–surface/ solvent-rich depletion layer developing if solvent has greater affinity for surface.

III. Adhesion (or True) Slip – fluid is in molecular contact with substrate and there is a breakage of bonds evidenced by relative tangential motion.

The first two mechanisms are "apparent slip". The third mechanism is the most vigorous violation of the no-slip condition since slip arises from bond-breaking. It is likely that cohesive slip – disentanglement between bulk and surface chains - most closely describes the interfacial slip in this study.

If slip occurs, the strain that the polymer actually "feels" is less than the applied strain. Brochard-Wyart and de Gennes [23] define the slip length, b, as the distance into the stationary substrate where the extrapolated velocity profile vanishes (Figure 1.1).

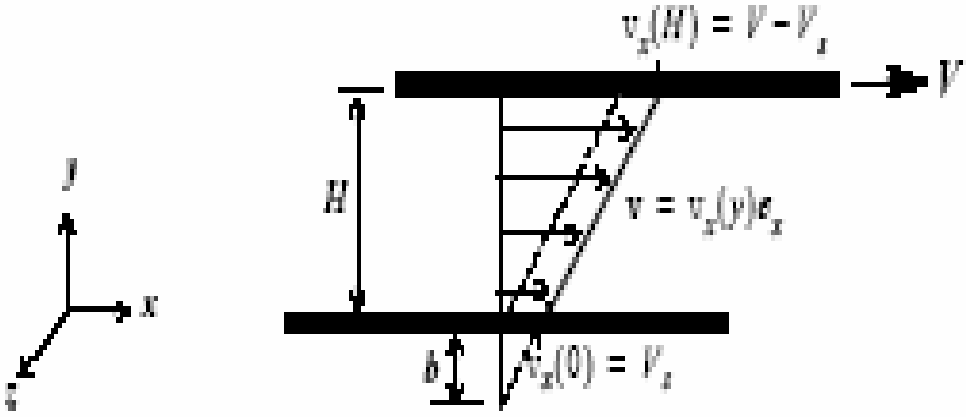

Figure 1.1: Definition of Slip Length, b

Ideally, both b and the slip velocity, V_s are zero at a stationary surface. So, non-zero values of either of these indicate the presence of an underlying mechanism, such as interfacial slip.

There is an abundance of reliable data, obtained via a myriad of techniques, quantifying interfacial slip in entangled polymers. Among the experimental methods are fluorescence recovery after photobleaching (FRAP) [24], using tracers to follow fluid flow and gap dependent measurements in torsional shear flow [25]. Therefore, unlike the case of shear banding, there can be little doubt that slip occurs in entangled polymers.

Since at high shear rates, polymers become prone to flow instabilities, a limiting shear rate might be reached before slip can be macroscopically detected. Also, if b (typically of order 1-1000 μm for polymers) << H, the onset of slip might be barely detectable making it difficult to characterize its critical conditions. So, direct visualization near the interface is ideal for characterizing slip.

The shear banding and interfacial slip discussion above outlines the challenges that must be surpassed or at least better understood, in nonlinear rheology of linear, entangled polymers. Another area where the D-E theory is apparently limited is in predicting flow in polymers with non-linear architectures. However, the only "requirement" of the original theory is that the chains are long enough to entangle, which means that entangled, branched polymers should also fall under its purview. In fact many commercially important polymers, like branched LDPE (low density polyethylene), are nonlinear. An interesting question is how these systems behave in non-linear rheology and whether they are susceptible to the same flow instabilities. Finally, the opposite case to the D-E polymer is an unentangled Rouse chain. In these systems the Rouse model [26] is the most appropriate choice; but, unlike the D-E theory, verification of this model has not been extensively studied.

In an effort towards resolving some of the lingering issues addressed in this chapter, a

summary of the studies performed throughout this work is as follows:

(1) For a series of linear polymers, step shear experiments are used to characterize the experimental damping function: $h_{exp}(\gamma) = G(t, \gamma)/ G(t, \gamma \rightarrow 0)$. The objective was to differentiate between shear banding and interfacial slip as causality factors for the D-E deviation called Type C Damping. Steady shear experiments were later (Chapter 3) done for the same systems used in the step shear study (Chapter 2). The polymers with $h_{exp}(\gamma)$ that agree with the D-E prediction are also well-behaved in steady shear experiments. The polymers that show Type C Damping are the only ones that give unexpected results in steady shear. Therefore we can easily make the connection between the step and steady shear experiments.

(2) For a series of entangled polymers, confocal rheology (confocal microscopy and particle image velocimetry) was used to do high resolution, shear profile measurements in a custom-built, planar Couette shear cell. The objective was to use this novel technique to determine whether shear banding is a general feature of entangled polymers (Chapter 3).

(3) The previous study (Chapter 3) was extended to include both transient velocity profile measurements and measurements at macroscopic shear cell gap sizes. The transient constitutive curve was also measured from start up to steady-state using mechanical rheometry. The objective was to determine whether a constitutive instability and/ or shear banded profiles is a transient state encountered during steady shearing of polymers and whether shear banding can be detected in a "slip-free" environment (Chapter 4).

(4) Linear viscoelasticity and nonlinear rheology (step shear) of entangled and unentangled star-branched polymers was investigated. The results were compared to predictions for both the Doi-Edwards and Rouse models (Chapter 5).

REFERENCES

1) P. G. De Gennes, J. Chem. Phys. **55**, 572 (1971).

2) M. Doi and S. F. Edwards, *The Theory of Polymer Dynamics* (Oxford, New York, 1986).

3) W. W. Graessley, Adv. Polym. Sci. **16**, 1 (1974).

4) E.V. Menezes and W.W. Graessley, J. Polym Sci B: Polym Phys **20**, 1817 (1982).

5) C. Pattamaprom and R. G. Larson, Macromolecules **34**, 5229 (2001).

6) V. R. Mhetar and L. A. Archer, J. Polym. Sci., Polym. Phys. Ed. **38**, 222 (2000).

7) M. Doi and S. F. Edwards, J. Chem. Soc. Faraday Trans. II **75**, 38 (1979).

8) N. A. Spenley, X.F. Yuan, and M.E. Cates, J. Phys.II France **6**, 551 (1996).

9) R. Makhloufi et al., Europhys. Lett. **32**, 253 (1995).

10) M. M. Britton and P.T. Callaghan, Phys. Rev. Lett. **78**, 4930 (1997).

11) T. C. B. McLeish and R.C. Ball, J. Polym. Sci. Polym. Phys. Ed., **24**, 1735 (1986); T. C. B. McLeish, J. Polym. Sci. Polym. Phys. Ed. **25**, 2253 (1987).

12) J. Yerushalmi, S. Katz, and R. Shinnar, Chem. Eng. Sci. **25**, 1891 (1970).

13) S. M. Fielding and P. D. Olmsted, Phys. Rev. Lett. **90**, 224501 (2003a); S. M. Fielding and P. D. Olmsted, Phys. Rev. E **68**, 036313 (2003b).

14) S. Kumar and R. G. Larson, J. Non-Newtonian Fluid Mech. **95**, 295 (2000).

15) R. S. Graham, A. E. Likhtman, and T. C. B. McLeish, J. Rheol. **47**, 1171 (2003).

16) J. F. Berret et al., *Europhys. Lett.* **25**, 521 (1994); J. F. Berret et al., *J. Physique* II **4,** 1261 (1994).

17) H. Rehage and H. Hoffmann, *Mol. Phys.* **74**, 933 (1991): 933; *J. Phys. Chem.* **92**, 4712 (1988).

18) N. A. Spenley, M. E. Cates, and T. C. B. McLeish, Phys. Rev. Lett. **71**, 939 (1993).

19) D. C. Venerus, J.Rheol. **49**, 277 (2004).

20) E. Schnell, J. Appl. Phys. **27**, 1149 (1956).

21) Y. X. Zhu and S. Granick, Phys. Rev. Lett**. 88**, 106102 (2002).

22) H. Hu. R. G. Larson and J. J. Magda, J. Rheol. **46**, 1001 (2002).

23) F. Brochard-Wyart and P.G. De Gennes, Langmuir **8**, 3033 (1992).

24) K.B. Migler, H. Hervet and L. L´eger, Phys. Rev. Lett**. 70**, 287 (1993)**.**

25) J. Sanchez-Reyes and L. A. Archer, Langmuir **19**, 3304 (2003).

26) P. E. Rouse, J. Chem. Phys. **21**, 1272 (1953).

CHAPTER 2

Cause of Type C Damping in Entangled Polymers: Shear Banding and Interfacial Slip

2.1 Introduction

2.1.1 Causes of Type C Damping

In step shear flow: $\gamma = \gamma_0 H(t)$, the D-E model [1] predicts that stress, $\sigma(\gamma, t)$ varies with strain in a universal manner for ALL entangled polymers:

$$\sigma(\gamma, t) = h(\gamma) * G(t) * \gamma \qquad \ldots(2.1)$$

where γ is step strain, $G(t)$ is the linear relaxation modulus and the function $h(\gamma)$ is called the damping function. The Doi-Edwards prediction for the damping function is:

$$h_{D\text{-}E}(\gamma) = (1+4/15*\gamma^2)^{-1} \qquad \ldots(2.2)$$

The experimental damping function (valid for $t > \lambda_k$, the time-strain factorability time) is:

$$h_{exp}(\gamma) = G(t, \gamma)/ G(t, \gamma \rightarrow 0) \qquad \ldots(2.3)$$

When compared to experimental data, the D-E predictions for polymers with weak to moderate entanglement densities (N/N_e) are quite accurate. This agreement of experimental data with theory is defined as Type *A* damping by Osaki [2].

For more highly entangled polymers, where the theory is expected to work best, $h_{exp}(\gamma)$ is more strain softening than $h_{DE}(\gamma)$. This effect is called type *C* damping [2] and was repeatedly observed in the work discussed hereforth (See Figures. 2.1 - 2.4)**.** More recent improvements and modifications [3-4] to the original tube theory are still unable to reconcile this deviation for polymers with high entanglement number. Type C Damping is thought to be due to one of three mechanisms: slip at the solid surface, edge fracture or constitutive instabilities (shear banding).

To be thorough, we mention that a fourth explanation – related to the torsional compliance time, τ_T of the rheometer transducer and the strain imposition time, t_{step} - was recently proposed as a cause of Type C Damping [5]. But, it is generally accepted that with short strain imposition time ($t_{step} < 0.1\ \tau_d$) and $\tau_T << \tau_{Rouse}$ (the fast retraction

time scale), these mechanical factors have negligible effect on stress relaxation measurements.

The stress relaxation modulus, G (t, γ), is measured using a cone & plate rheometer. For each polymer studied, a small-amplitude oscillatory shear test: storage and loss modulus (G' and G'') as a function of frequency, ω, was performed before and after each series of step shear strains. The fact that the before & after curves always overlapped is significant. We can be reasonably confident that edge fracture is not the cause of type C behavior because it is an irreversible process, which would affect the measured fluid properties.

Differentiating between shear banding and interfacial slip as causality factors for Type C Damping is much less straightforward. In fact, it is has been argued that slip is a type of shear banding [6], which makes it even more difficult to separate these two effects. In capillary flow of concentrated melts and polymer solutions, at some critical wall stress, theory predicts a separation of the polymer into two (low & high shear rate) regions [6]. Highly sheared polymer can then accumulate in a small region near the wall; if this happens, the resulting effect looks like "wall slip" experimentally.

It is also possible that shear banding is a precursor to edge fracture in cone & plate rheometry. This effect is related to the boundary conditions for the second normal stress difference ($N_2 = \sigma_{yy} - \sigma_{zz}$), which can differ for the two coexisting shear band regions [7]. Ignoring surface tension forces, this imbalance between atmospheric pressure, which is the same for both regions, and the outward normal stress, σ_{zz}, can lead to expulsion of sample from the gap.

It is clear that macroscopic techniques are insufficient for separating the factors that contribute to Type C Damping. Even non-rheometric methods like flow birefringence and neutron scattering only yield data spatially averaged over the entire gap. Focusing on interfacial slip and shear banding as the two most likely causes of

Type C behavior, we use particle image velocimetry in narrow-gap, planar-Couette steady shear flow (Chapters 3- 4) to carefully probe differences (if any) between layers in the gap. In our confocal microscopy set-up, we studied entangled polybutadiene solutions, which displayed Type C Damping in cone & plate macroscopic experiments. This will help us to isolate the underlying mechanism causing this effect.

2.1.2 Shear Banding and Type C Damping

In Type C deviations the applied deformation produces smaller stresses than expected. This effect can increase quite dramatically with an increase in entanglement density, Z ($Z = N/N_e$) (See Figure 2.2)**.** A theoretical explanation proposed by Marrucci and Grizzuti [8] says that on some microscopic length scale, the deformation of the polymer is non-homogeneous. Because of the predicted D-E stress $\{\sigma(\gamma, t) = G(t, \gamma)^* \gamma\}$ maximum, at sufficiently high γ, the deformation may not be stable. Upon strain imposition, a very fast separation occurs with adjacent fluid layers having different magnitudes of shear. After a while, the instability disappears, and the stress relaxes from this non-uniform deformation in a normal way.

Marrucci-Grizzuti proposed that it is only at the end of the fast relaxation stage that this instability can arise. According to the theory, the relative rate of the fast and slow stress relaxation processes determines the deformation instability criterion. The criterion says that non-uniform deformation is most favored when only a very small fraction of chains, χ, are back to the isotropic state after the first relaxation stage [8]. This fraction depends on the ratio of the slow to fast relaxation time scales and hence depends on N. Therefore χ is smaller for polymers with higher entanglement density, Z. The large reptation/retraction time scale ratios associated with highly entangled,

monodisperse polymers makes them more prone to Type C behavior and might also explain why deviations increase with Z. Some experimental evidence appears to support this Marrucci-Grizzuti theory [9]. But, the exact structure of this flow-induced strain inhomogeneity cannot be detected macroscopically, which underscores the utility of our microscopic measurement technique (Chapters 3 - 4).

There is similarity between the polymers (PBD solutions) and experimental technique (velocimetry in couette geometry) presented in Chapters 3-4 and recent work by Hu et al. and Wang et al. [10-12]. Because of this, that work is discussed in some detail in the section below.

2.1.3 Previous Work – Shear Banding

To probe the steady-state flow behavior of monodisperse, entangled polybutadiene (PBD) solutions more carefully, Hu et al [10] constructed the constitutive curve using local shear rates. The local shear rate was extracted from the measured velocity profile and the predicted (based on geometry) local stress was used. The authors used a particle tracking velocimetry (PTV) set-up coupled to a rheometer with couette, co-cylinder: CO 35-34 mm fixtures [13]. A laser light beam illuminated a cross section of the polymer sample, which was seeded with 10 μm silver coated spherical particles, in the x-y plane. During shear, an image of the entire gap was collected at 90° to the illumination plane by a charge coupled device (CCD) camera underneath the cell. They also coupled the PTV set-up to a cone & (walled) plate (CP40-2.65°) geometry. One key advantage of our planar- Couette geometry experiments (Chapters 3-4) over the co-cylinder geometry is that there is no stress gradient.

For all the PBD solutions (with Z up to about 47) studied, these authors found

only linear velocity profiles in the Newtonian shear rate region. For rates in the non-Newtonian regime ($\dot{\gamma} > \tau_d^{-1}$), no steady state shear banding was detected. In addition to the monotonic constitutive curve plotted from directly measured local shear rates, the non-banded velocity profiles provide further support of a monotonic constitutive relation.

Another group – Wang et al [12] got different results using a polymer nearly identical to the Z = 47 PBD solution studied by Hu et al [10]. Wang et al used the same PTV-cone & plate set-up (but with CP25-5°). The measurement gap was 0.9mm and they studied the velocity profile for three different applied shear rates corresponding to the Newtonian, just before stress plateau and well inside the stress plateau regions of the constitutive curve. For the highest applied rate, a curved profile developed gradually: at start up the profile is linear, and then curved in both the transient (i.e. the stress downturn region after the overshoot) and steady state regions.

This evolution was also observed by Hu et al but differs in that Hu only found transient shear banding. The 'banded' profile became linear at times, which were well into the steady state region. In contrast, the curved transient profile seen by Wang et al persisted even at steady state. It is possible that Wang's result (curved profiles) might be reflective of not waiting long enough for "true" steady state. The authors also speculated that the curved profiles was a result of polymer polydispersity (M_w/M_n=1.18 for the PBD melt) and set out to test this hypothesis [11].

In this next set of experiments [11], a monodisperse (M_w/M_n=1.02, Z = 18) solution was loaded into a sliding plate rheometer; the bottom plate was fixed and the upper one moved by a stepper motor. A laser beam shone through a small slit in the top plate illuminated the sample and an image of the entire gap was captured by a CCD camera. When sheared in the non-Newtonian regime, the profile is linear at short times but two distinct shear bands emerge at transient times and continue at "steady

state". However, these experiments were not done far enough into the steady state region; so, we note the possibility that the observed shear banding may in fact disappear at longer times (as observed Hu et al [10]).

According to Cates at al's modified D-E theory, for Couette flow within the unstable region, shear stress is constant and there can be only two values of shear rate [7]. So, varying the plate speed (applied shear rate) only varies the relative proportion of highly sheared material. However, in Wang's sliding plate rheometer experiments, the shear rate of the fast band increased with applied rate while its width stayed the same – an observation not consistent with theory. This suggests that something other than a non-monotonic constitutive curve, such as shear enhanced concentration changes, could be the cause of the shear banding found by this group. Further work is needed to probe mechanisms causing anomalous flow during steady shear of these entangled polybutadienes, which justifies this work.

2.1.4 Previous Work – Interfacial Slip

Prior to the current study there have been multiple attempts to characterize interfacial slip. In one significant work, Mhetar and Archer [14] used particle velocimetry to study slip in narrow molecular weight distribution (MWD) polybutadiene melts (Z = 31 - 239). The polymers, imbedded with silica tracer particles (1.5 μm diameter), were sheared over glass surfaces in plane-Couette flow. The bottom glass plate of the shear cell was held on a roller slide, which was connected to a force transducer for stress measurement. The top glass plate was connected to a micro-stepper motor. The gap between the two plates was 250-500 μm. The displacement of the particles from their initial resting place was measured by a video camera interfaced with a time lapse

recorder.

For the least entangled melts in the series, $V_s \sim \sigma$ over the entire range of shear stresses; so, that the slip length was constant. For the others ($Z \geq 60$), three distinct slip regimes were observed: weak slip ($\sigma < \sigma^*$): b = 10-150 μm, intermediate stick-slip ($\sigma \approx \sigma^*$) and strong slip ($\sigma > \sigma^*$): b ~ 100-1500μm, where σ^* is some critical stress

2.2 Materials and Experiment

2.2.1 Polybutadiene and Polyisoprene

Entangled solutions made from linear, narrow molecular weight distribution (MWD) 1, 4- polybutadiene melt was chosen as the main polymer for this study for a few reasons. First, the low glass transition temperature, T_g = -78 °C [15] of PBD allows us to do experiments at room temperature. Second, PBD has a low entanglement molecular weight (M_e=1822 g/mole) [16]. This means that even low concentration solutions can be highly entangled, which allows us to study the effect of changing N/N_e (Z). Third, these polymers are not only readily commercially available, but we also have the facilities to make them in our lab. Fourth, with suitable hydrogenation, polybutadiene is chemically similar to polyethylene. The latter is an important polymer in extrusion processes, where surface instabilities (caused by factors like interfacial slip) cause extrudate defects.

Solutions of linear 1, 4 – polyisoprene (PI), which also has low T_g and fairly low M_e = 4200 g/mole [17], were also studied. Compared to PBD, there is a relative shortage of non-linear rheology data for polyisoprene. Additionally, a step shear study of both polymers allows us to investigate whether Type C Damping effects are polymer- specific. The properties of all the polymer solutions are shown in Table 2.1

(φ is the melt concentration). The longest relaxation time, τ_d, is the reciprocal of the shear frequency at which $\eta''(\omega)$ manifests a global maximum. The plateau modulus, G_N, is the storage modulus $G'(\omega)$ at which *tan*δ manifests a global minimum in the high-frequency rubbery viscoelastic regime.

2.2.2 Polymer Synthesis

Both PI 250 K ($M_w/ M_n = 1.01$) and PBD 200K ($M_w/ M_n = 1.05$) melts were synthesized "in-house" via high vacuum anionic polymerization. PBD 788K ($M_w/ M_n = 1.1$) was purchased from Polymer Source Inc. In the first step of PI synthesis, degassed isoprene monomer and cyclohexane solvent were purified using N-butyl lithium initiator. The "clean" products were then distilled into a reaction vessel attached to the vacuum line. Next, the monomer was initiated by *sec*-Butyl lithium under ambient (O_2, H_2O free) conditions inside a glove box (M-Braun Inc.). After a few days, the living polymer chains were terminated with degassed isopropanol.

The PBD synthesis procedure is similar but is complicated by the fact that the monomer is gaseous at room temperature. The butadiene monomer purification is carefully done at sub-zero temperatures in a reaction vessel surrounded by an isopropanol/ dry ice bath. Both polymers were characterized by gel permeation chromatography (GPC); PI 250K was also characterized by SEC [17].

Table 2.1: Properties of PI 250 K, PBD 200 K and PBD 788K solutions

	N/ Ne	τ_d *(s)*	G_N *(Pa)*
PI 250 K, φ= 0.3	11	0.4	$2.05*10^4$
PI 250 K, φ= 0.4	17	0.63	$5.87*10^4$
PI 250 K, φ= 0.6	30	1.26	$1.53*10^5$
PI 250 K, φ= 0.7	37	1.59	$1.91*10^5$
PI 250 K, φ= 0.8	44	1.99	$3.14*10^5$
PBD 200K, φ = 0.4	32	0.79	$2.20*10^5$
PBD 200K, φ = 0.6	56	1	$5.11*10^5$
PBD 200K, φ = 0.8	82	1	$8.63*10^5$
PBD 788K, φ = 0.05	8	2.7	$1.3*10^3$
PBD 788K, φ = 0.1	20	11.9	$7.5*10^3$
PBD 788K, φ = 0.2	51	31.6	$4.49*10^4$

2.2.3 Mechanical Rheometry

Step shear and small-amplitude oscillatory shear experiments were done at 28 °C using a Rheometric Scientific-LS (ARES) rheometer and an Anton Paar Physica Modular compact rheometer (MCR 300). The cone and plate fixtures used were – CP 25mm -5.7°, CP 10 mm - 5.4° and CP 6 mm - 4.9°.

2.3 Results and Discussion

We performed step shear experiments for the entire set of PI 250 K solutions (φ=0.3, 0.4, 0.6, 0.7, 0.8), PBD 200K solutions (φ=0.4, 0.6, 0.8) and PBD 788K solutions (φ=0.05, 0.1, 0.2). A series of step strain deformations (ranging from γ= 0.1- 5.01) was applied and G (t, γ) measured. The experimental damping function for each solution is calculated according to Eq. (1.3), and then compared to theory (Figures 2.1-2.4). h_{exp} (γ) is evaluated at the chain disengagement time: $t = \tau_d$. τ_d is larger than the factorability time since h_{exp} (γ) is independent of time when evaluated at $t > \tau_d$.

The polyisoprene solutions gradually transition to Type C Damping as entanglement number increases (Figure 2.1). We observe both Type A (φ=0.3, 0.4) and Type C Damping (φ=0.7, 0.8). The solution with the lowest φ (and hence lowest Z) displays the rarely reported behavior called Type B Damping - a weaker strain dependence than D-E [2].

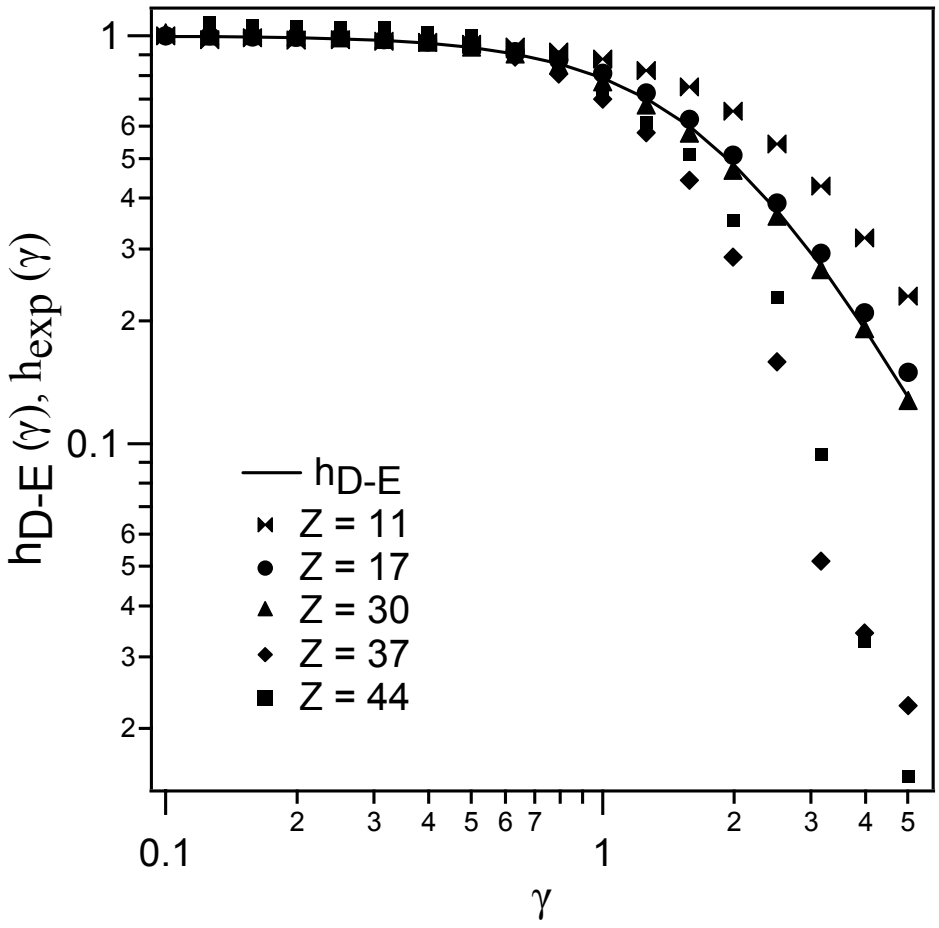

Figure 2.1: Damping functions for PI 250 K solutions

There are no molecular theories that fully explain Type B behavior. We can qualitatively understand Type B damping by considering the effect of low Z. The entanglement interaction is due to the stipulation that chain contours cannot cross each other [18]. In a system with fewer entanglements, more paths are available for configurational (tube) relaxation than in one with more topological constraints. So, it is likely that the D-E tube model is not as valid for the φ=0.3 polymer solution. In the extreme case of an un-entangled polymer, the Rouse Model [19] predicts that the damping function is completely γ-independent. This might explain the transition to weaker strain dependence for this moderately entangled polymer.

Unlike the PI solutions, the polybutadiene 200K solutions all show Type C Damping (Figure 2.2) and D-E deviations increases with Z. Another interesting observation is that, for most of the solutions (both PIs and PBDs), maximum deviations: $\left| h_{DE}(\gamma) - h_{exp}(\gamma) \right|$ occur at intermediate strains. This suggests a transition from Type C to Type A Damping at large strains. $\left| h_{DE}(\gamma) - h_{exp}(\gamma) \right|$, which indirectly quantifies the severity of the mechanism causing Type C Dmaping, increases with γ then decreases after reaching a maximum.

This finding does not help much in differentiating between interfacial and shear banding since it is consistent with both. The behavior is at least qualitatively consistent scaling model for slip proposed by Mhetar et al. [14]. In this model, the variation of V_s - a direct measure of slip- with an applied stress (strain) is also quadratic in nature: $V_s \sim \sigma^{2.1}$. However, the decreasing deviations might also be explained by the shear banding arguments outlined in section 2.2: one stress level [G (t, γ)/ G (t)] corresponding to two distinct γ.

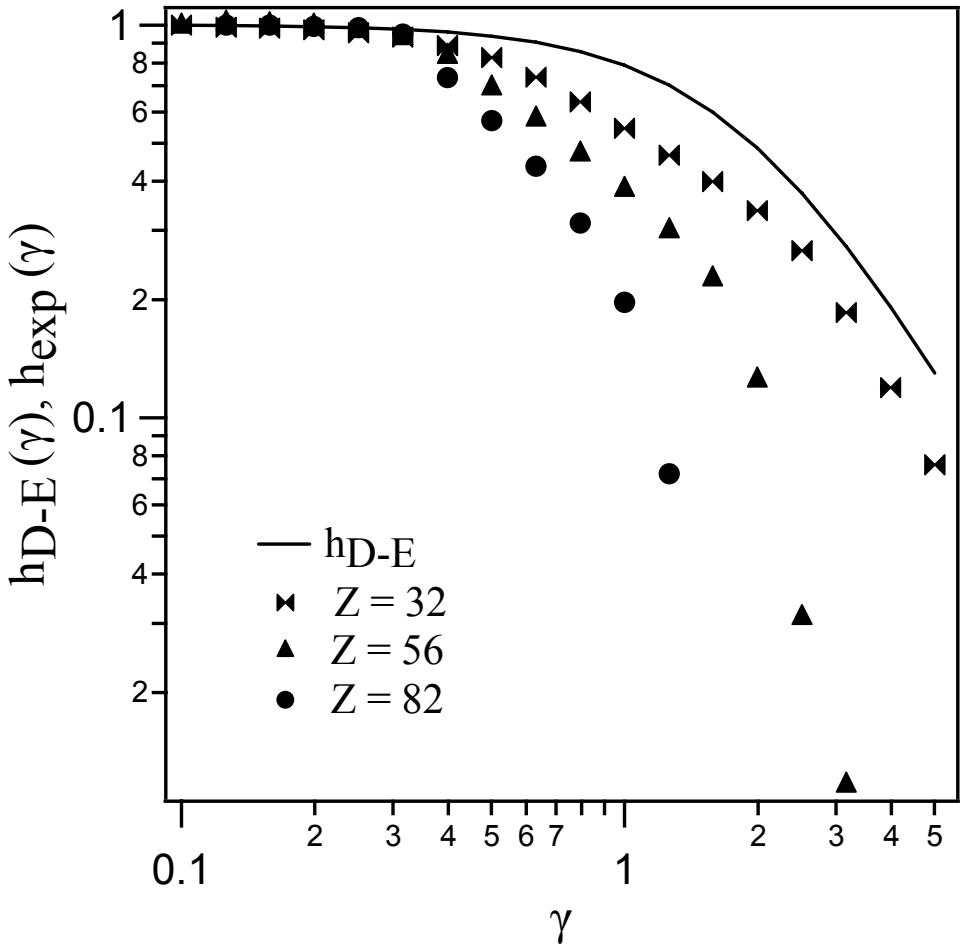

Figure 2.2: Damping functions for PBD 200 K Solutions

The data reveals slightly different behavior for polyisoprene and polybutadiene. When $h_{exp}(\gamma)$ of a PI 250K solution (φ=0.6) is compared to $h_{exp}(\gamma)$ for a PBD 200K (φ=0.4) solution with similar number of entanglements (Figure 2.3)**,** the former agrees with theory while the latter shows Type C Damping. Previous experiments [20] suggest that the damping function does not only depend on γ, but that it is also affected by Z. A similar conclusion could be reached from our data (Figure 2.1). However, PBD appears to be much more prone to Type C Damping: lower critical Z for Type A to Type C transition and larger $\left| h_{DE}(\gamma) - h_{exp}(\gamma) \right|$ than PI. For the PBD 788K solution series (Figure 2.4), two solutions follow the D-E prediction while the most entangled (Z = 51) shows Type C Damping deviations.

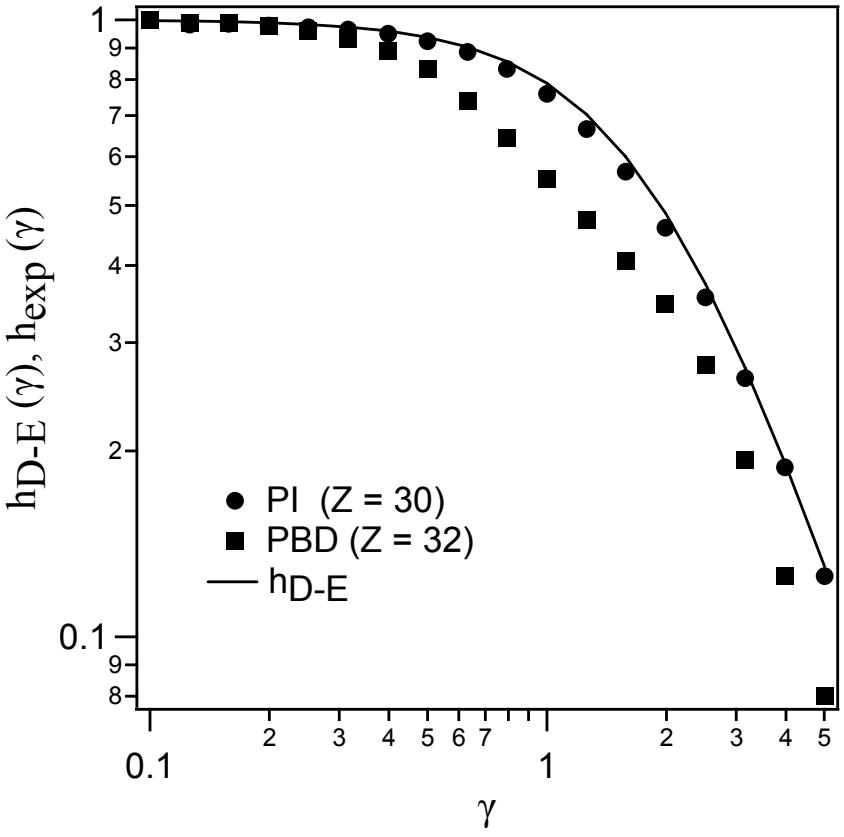

Figure 2.3: Comparison of D-E deviations for PBD 200K and PI 250K solutions with similar Z

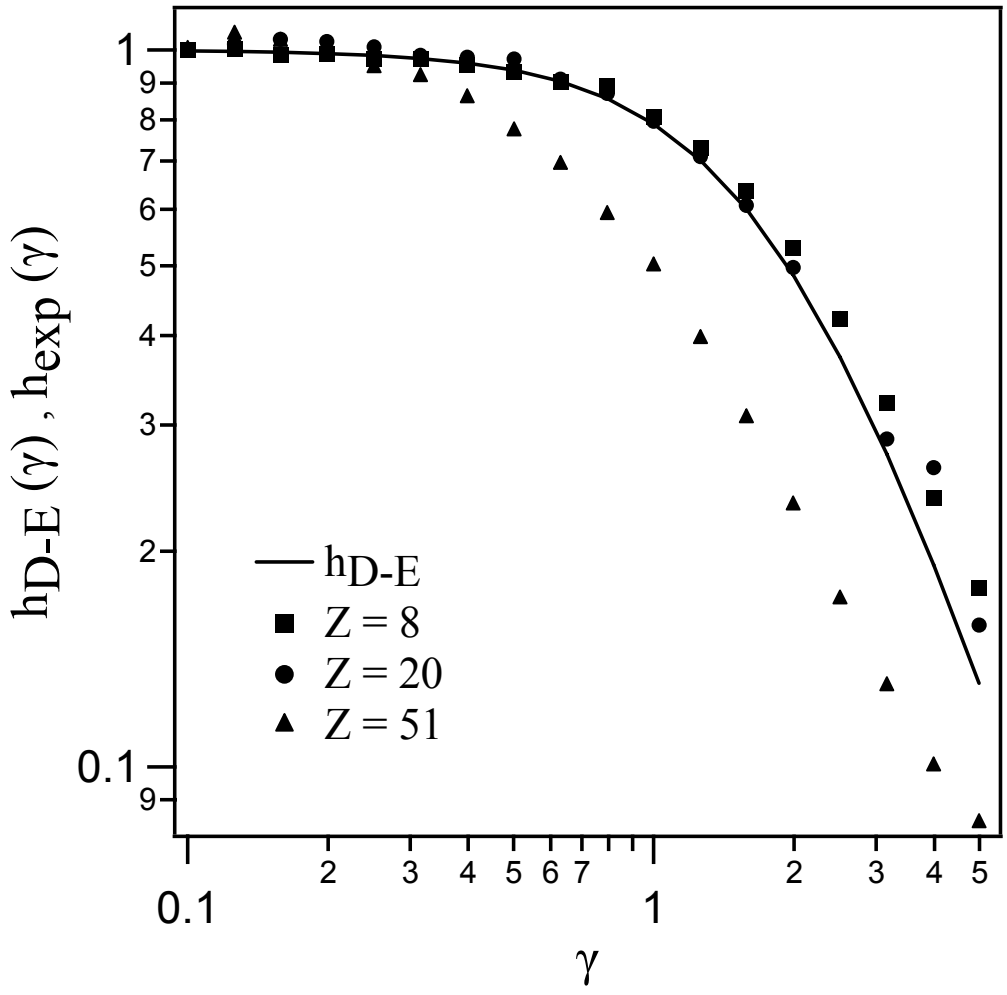

Figure 2.4: Damping functions for PBD 788 K solutions

2.4 Conclusion

Both the polyisoprene and polybutadiene solutions show Type C Damping deviations that become larger with increasing entanglement number. There is also a Type C to Type A Damping transition at the larger strains. Type C Damping in the polybutadiene solutions is much more severe than that for polyisoprene solutions with comparable entanglement densities. It is entirely possible that the Type C Damping behavior seen on the macroscopic scale has contributions from both interfacial slip and constitutive instabilities. However, conventional rheometry is insufficient for resolving this issue. A different technique, which can directly visualize flow in the gap, is needed.

An investigation which uses this technique to measure flow in both Type A and Type C Damping polymers will illuminate the cause of Type C deviations. When this method is used to study 'Type A' polymers, the experimental results should match expected values, as they do in step shear flow.

REFERENCES

1) M. Doi and S. F. Edwards, *The Theory of Polymer Dynamics* (Oxford, New York, 1986).

2) K. Osaki, *Rheol. Acta **32***, 429 (1993).

3) D.W. Mead, R. G. Larson, and M. Doi, Macromolecules **31**, 7895 (1998).

4) M.T. Islam and L.A Archer, J Polym. Sci., Polym. Phys. Ed **39**, 227 (2001).

5) D. C. Venerus, J. Rheol. (N.Y.) **49**, 277 (2004).

6) T. C. B. McLeish and R.C. Ball, J. Polym. Sci. Polym. Phys. Ed., **24**, 1735 (1986); T. C. B. McLeish, J. Polym. Sci. Polym. Phys. Ed. **25**, 2253 (1987).

7) M. E. Cates, T. C. B. McLeish, and G. Marrucci, Europhys. Lett. **21**, 451 (1993).

8) G. Marrucci and N. Grizzuti, J. Rheol. **27**, 433 (1983).

9) F. Morrison and R. G. Larson, J. Polym. Sci., Polym. Phys. Ed. **30**, 943 (1992).

10) Y. T. Hu and L. Wilen, J. Rheol. (N. Y.) **51**, 275 (2007).

11) P. E. Boukany and S. Q. Wang, J. Rheol. (N. Y.) **51**, 217 (2007).

12) P. Tapadia and S. Q. Wang, Phys. Rev. Lett. **96**, 016001 (2006).

13) Y. T. Hu and A. Lips, J. Rheol. **49**, 1001 (2005).

14) V. R. Mhetar and L.A. Archer, Macromolecules **31**, 8607 (1998).

15) J. D. Ferry, *Viscoelastic Properties of Polymers* (John Wiley, New York, 1980).

16) Juliani and L. A. Archer LA, J Rheol **45**, 691 (2001).

17) J. H. Lee et al., Macromolecules **39**, 6677 (2006).

18) W. W. Graessley, Adv. Polym. Sci. **16**, 1 (1974).

19) P. E. Rouse, J. Chem. Phys. **21**, 1272 (1953).

20) M. T. Islam, J. Sanchez-Reyes, and L. A. Archer, J. Rheol. **45**, 61 (2001).

CHAPTER 3

High Resolution Shear Profile Measurements in Entangled Polymers*

***Reproduced with permission from: Physical Review Letters, Vol. 101, 218301**

Keesha A. Hayes, Mark R. Buckley, Itai Cohen, Lynden A. Archer

3.1 Summary

We use confocal microscopy and particle image velocimetry to visualize motion of 250-300 nm fluorescent tracer particles in entangled polymers subject to a rectilinear shear flow. Our results show linear velocity profiles in polymer solutions spanning a wide range of molecular weights and number of entanglements ($8 \leq Z \leq 56$), but reveal large differences between the imposed and measured shear rates. These findings disagree with recent reports that shear banding is a characteristic flow response of entangled polymers, and instead point to interfacial slip as an important source of strain loss.

3.2 Introduction

Flow properties of entangled polymers are important in myriad commercial processes used for molding, extruding, and spinning plastic components. The Doi-Edwards (D-E) theory provides the most successful molecular framework for understanding these properties. Developed around the reptation or "tube" model [1], this theory contends that a melt of entangled polymers responds affinely to instantaneous macroscopic deformations. The affine response is sustained by long-lived entanglements between molecules and causes the network of entanglements (tube) confining any given molecule to orient and stretch in the same way as does the macroscopic melt. Polymer molecules trapped in the tube initially stretch and orient in synergy with their environment.

D-E predictions for step strain, oscillatory and steady shear flows agree, sometimes quantitatively, with experiments [2-6]. A more controversial prediction is that under steady shear, the shear stress is a multi-valued function of the imposed shear rate. Thus, simple shear flow is unstable to perturbations in shear rate and should produce shear banding [7, 8]. Surprisingly, with the exception of entangled worm-like micellar fluids [9-11], banding is generally not observed in flows of entangled polymers at any shear rate. This implies that some other dynamic processes not taken into account by the theory must contribute to the fluid's response. Efforts to date have focused on understanding how convective acceleration of reptation [12-17], tube diameter shrinkage [18], and slip [19-22] near the shearing surfaces influence this prediction. All three processes eliminate or weaken the driving force for entangled polymers to shear band, and when integrated into the D-E theory, lead to steady shear stress predictions that compare favorably with experiments using moderately

entangled polymers.

Recent velocity profile measurements using 10μm silvered particles dispersed in entangled polybutadiene solutions show, for the first time, that entangled polymer systems do in fact appear to shear band [23-25]. Surprisingly, these studies find that shear banding occurs even in solutions with intermediate levels of entanglements, generally thought to be well-described by D-E theory with the aforementioned modifications. Parameters such as shear strain and shear rate, widely used to characterize shear of entangled polymers, are ill-defined in a banded fluid, implying that all published nonlinear rheological data on these systems are challenged by the recent findings. Establishing whether these recent observations of banding are generally applicable to polymers in the class of entangled fluids is therefore of critical significance to the field [26].

In this study we report on a technique that incorporates fast confocal microscopy to investigate flow of entangled polybutadiene solutions. This technique has previously been shown to accurately detect shear banding in colloidal suspensions on the micron scale [27]. We apply it to analyze rectilinear shear flow between parallel planes because this geometry has multiple inherent advantages over the more commonly used Couette and cone-and-plate geometries. First, the absence of curvature in material lines makes interpretation of the velocity profile straightforward. Second, polymeric materials are not susceptible to any of the plethora of hydrodynamic, elastic, and edge effects that plague fast flow experiments of these liquids [28-29, 30-31]. Additionally, for low enough gap (plane separation, H) to width (W) ratios $H/W = a_s<1/50$, weaker secondary flows induced by normal stresses are suppressed [32]. Finally, the temperature rise (ΔT) produced during shear of a low thermal-conductivity (k) polymer fluid can have profound effects on the velocity

profile in any flow geometry [33]. For our flow geometry, $\Delta T = \frac{\sigma\dot{\gamma}}{k}H^2$, where σ and $\dot{\gamma}$, are respectively the shear stress and shear rate. Thus, provided the gap is small, flow anomalies produced by viscous heating can be minimized. The experiments we report are performed in a custom-built shear cell with $a_s \leq 1/143$ and H = 25-35 μm; both are at least one order of magnitude lower than is typical for polymer flow experiments. Our device therefore provides an essentially ideal setting for investigating banding in entangled polymer flows. Remarkably, we find that the measured velocity profiles are generally linear even for shear rates well into the non-Newtonian flow regime.

According to the D-E theory, the shear rates at which shear stress $\sigma_{yx} \equiv \sigma_s$ (flux of momentum normal to the flow direction, x), is multi-valued are related to the microscopic relaxation mechanisms accessible to polymers within their local tubes. At low rates, $\dot{\gamma} < \tau_{rept}^{-1}$, polymer chains escape their surroundings by reptation, essentially unperturbed by the shear. As a result, momentum is transferred by secondary interactions and entanglements between randomly oriented molecular units, leading to a simple viscous response. For shear rates $\dot{\gamma} \geq \tau_{rept}^{-1}$, chains can slip within their affinely deforming tubes to preserve their equilibrium length, but cannot otherwise escape the tube constraint. Consequently the trapped chains orient in the direction of shear, yielding progressively less efficient momentum transport between fluid layers as shear rate increases. The resultant steady-state σ_s–shear-rate relationship can be expressed analytically,

$$\sigma_s(\dot{\gamma} \ll \tau_{Rouse}^{-1}) = \int_{-\infty}^{t} \sigma_s(\{t-t'\}, \dot{\gamma}\{t-t'\})dt' \approx \frac{15}{4}\dot{\gamma}\tau_{rept}G_e / [1+\frac{4}{15}(\dot{\gamma}\tau_{rept})^2], \quad (3.1)$$

and manifests a maximum at $\dot{\gamma} = \sqrt{15/4}\tau_{rept}^{-1}$. Here G_e is the elastic or *plateau* modulus

of the polymer. The D-E theory predicts that shear alignment continues until $\dot{\gamma}\tau_{Rouse} \geq 1$, at which point polymer chains begin to deform/ stretch in sympathy with their surroundings. Chain stretch makes a contribution $\dot{\gamma}\tau_{Rouse}G_N$ to σ_s, which arrests the down-turn in σ_s (Figure 3.1). In the multivalued regime, $\sqrt{15/4}\tau_{rept}^{-1} \leq \dot{\gamma} < \tau_{Rouse}^{-1}$, the material therefore forms two bands, each characterized by different shear rates and distinct relaxation processes.

3.3 Materials and Experiment

To characterize the velocity profile, $v(y)$, 250-300nm functionalized silica tracer particles, which encapsulate the fluorophore tetramethyl rhodamine isothiocyanate in were dispersed in entangled polybutadiene (PBD) solutions. The average number of entanglements, Z, was varied by changing the volume fraction of two high-molar-mass polymers: $\bar{M}_w = 7.9\times10^5\, g/mol$, $\bar{M}_w/\bar{M}_n = 1.1$ (PBD788K, Polymer Source Inc.) and $\bar{M}_w = 2\times10^5\, g/mol$, $\bar{M}_w/\bar{M}_n = 1.05$, (PBD200K, synthesized in-house) in an un-entangled PBD host, $\bar{M}_w = 1\times10^3\, g/mol$. The seeded solutions were sandwiched between glass planes maintained at separation H between 25 μm and 35μm. The plates were integrated into a motorized planar-Couette shear cell, which fits on the sample stage of a Zeiss 5-Live inverted confocal microscope equipped with a 100 X objective and 120 fps maximum capture rate. Because the tracer particles are substantially smaller than ones used previously [23-26], the velocity profile can be probed on a finer scale.

To generate shear flow in the polymer, one plane is moved relative to the other at a prescribed velocity $V\boldsymbol{e}_x$ using a controlled-speed inchworm motor (Burleigh – TSE 820). The nominal shear rate, $\dot{\gamma}_{nom} = V/H$, is varied by adjusting V and the shear

force, F_s, measured using a single-point load cell (S300, Strain Measurement Devices Inc.). The entire velocity profile is characterized, one layer at a time (typically 3 μm apart), using the confocal microscope to scan two-dimensional micrographs. To construct the profile, we simultaneously monitor $\sigma_s(t) = F_s(t)/W^2$ versus time and record the time-dependent particle motions in a given layer. A modified version of MATPIV is used to extract the displacement values. At steady state, defined here as the time at which σ_s and the tracer velocity cease to vary with time, the average particle velocity in that layer is determined. This process is repeated layer-by-layer until the entire profile is characterized.

3.4 Results and Discussion

Figure 3.1 reports baseline steady-state shear stress-versus shear rate data for all polymers used in the study, obtained using an ARES controlled-strain rotational rheometer with cone-and-plate fixtures. The solid line in the figure is the prediction of Eq. (3.1) for a polymer with $Z = 20$. For the PBD200K solutions, σ_s and $\dot{\gamma}$ are non-dimensionalized using the respective *plateau moduli* $G_N \approx G_e$ and *disengagement times* $\tau_d \approx \tau_{rept}$ deduced from linear viscoelasticity (LVE) measurements. For the PBD788K solution the shear rate is non-dimensionalized using τ_d, but the shear stress requires a value $G_e = 1.8\times10^3 Pa$, which is about twenty-five times lower than G_N, to yield a stress-versus-rate curve consistent with the other fluids. This last observation is unusual for an entangled polymer solution, but has been confirmed using the frequency-dependent complex modulus G^* data (open squares). Additionally, these

G_N values have been compared with G_{N0} for the PBD788K melt to verify the solution concentration, $\phi = (G_N / G_{N0})^{3/7}$.

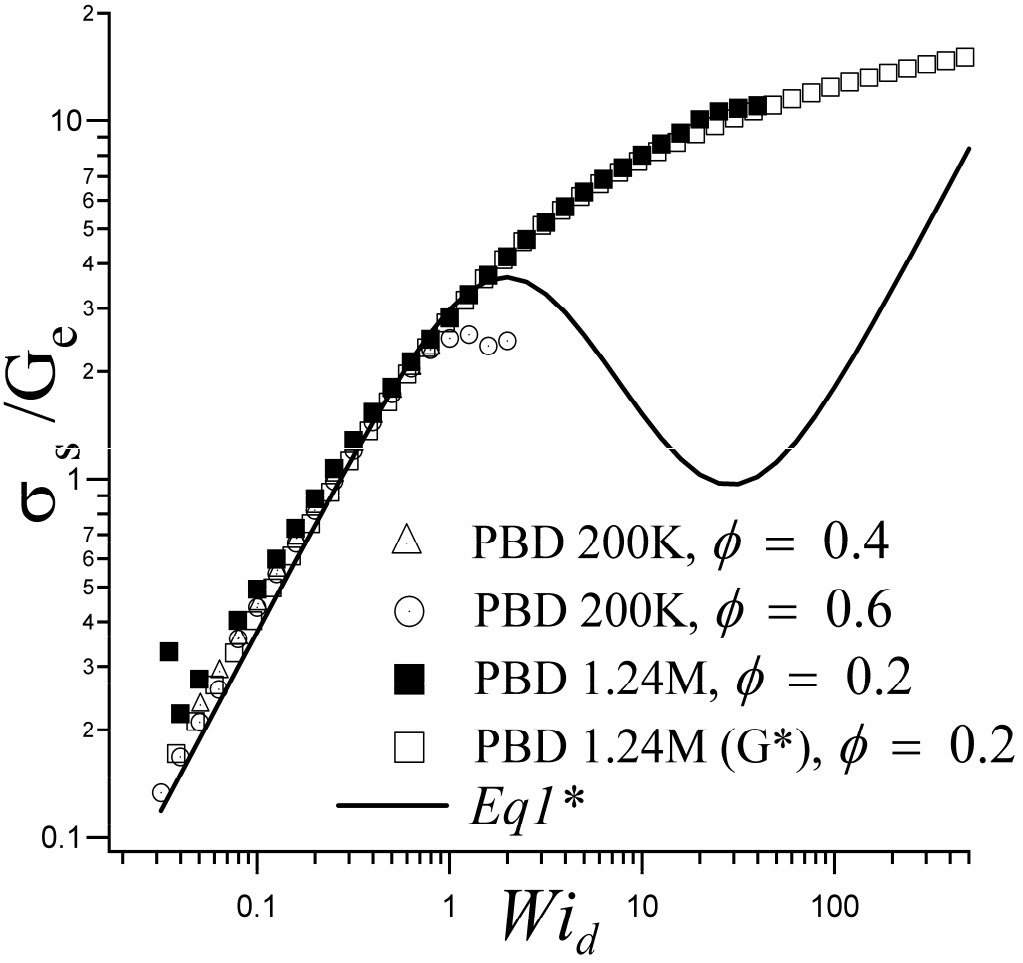

Figure 3.1: Dimensionless steady-state shear stress versus dimensionless shear rate for PBD solutions.

Figure 3.1 shows that most features predicted by the D-E theory for $\dot{\gamma} < \tau_d^{-1}$, including the universal relationship between σ_s / G_e and the dimensionless shear rate, $Wi_d \equiv \dot{\gamma}\tau_d$, are consistent with the experimental data. At higher shear rates, both PBD200K solutions display stress plateau regimes. However, data in this flow regime is limited because σ_s displays erratic time-dependent behavior and consistent steady-state values could not be obtained. This behavior is observed in a Wi_d range where the D-E model manifests the aforementioned multivalued behavior, implying either that the shear flow is unstable to shear-banding or that other phenomena, e.g. slip or viscous heating, compromise the measurements. This should be contrasted with σ_s versus Wi_d for the PBD788K solution, which shows no evidence of a plateau.

Figures 3.2-3.6 provide a sample set of velocity profiles at shear rates spanning the simple shear, $\dot{\gamma} < \tau_d^{-1}$, banded shear flow, and high-shear stable shear flow, $\dot{\gamma} > \tau_{Rouse}^{-1}$ predictions of the D-E theory. Z ranges from 8 to 56, and the shear viscosity differs by more than three orders. The true shear rate, $\dot{\gamma}_T$, corresponding to the line slope m, and $\dot{\gamma}_{nom} = (V/H)_{nom}$ are provided in each case. It is apparent from that the velocity profiles are in most cases fitted quite well by straight lines, showing no evidence of banding. Indeed at the highest shear rates in Figures 3.4 and 3.5, $\dot{\gamma}\tau_d = 5.8$ and 27, the profiles are decidedly linear. These shear rates are well into the non-Newtonian flow regime (Figure 3.1) and substantially above those where shear banding is expected. Surprisingly, a solution with a comparable level of entanglement to PBD788K with $\phi = 0.1$ was shown by Tapida et al. [23] to shear band, which is inconsistent with our measurements.

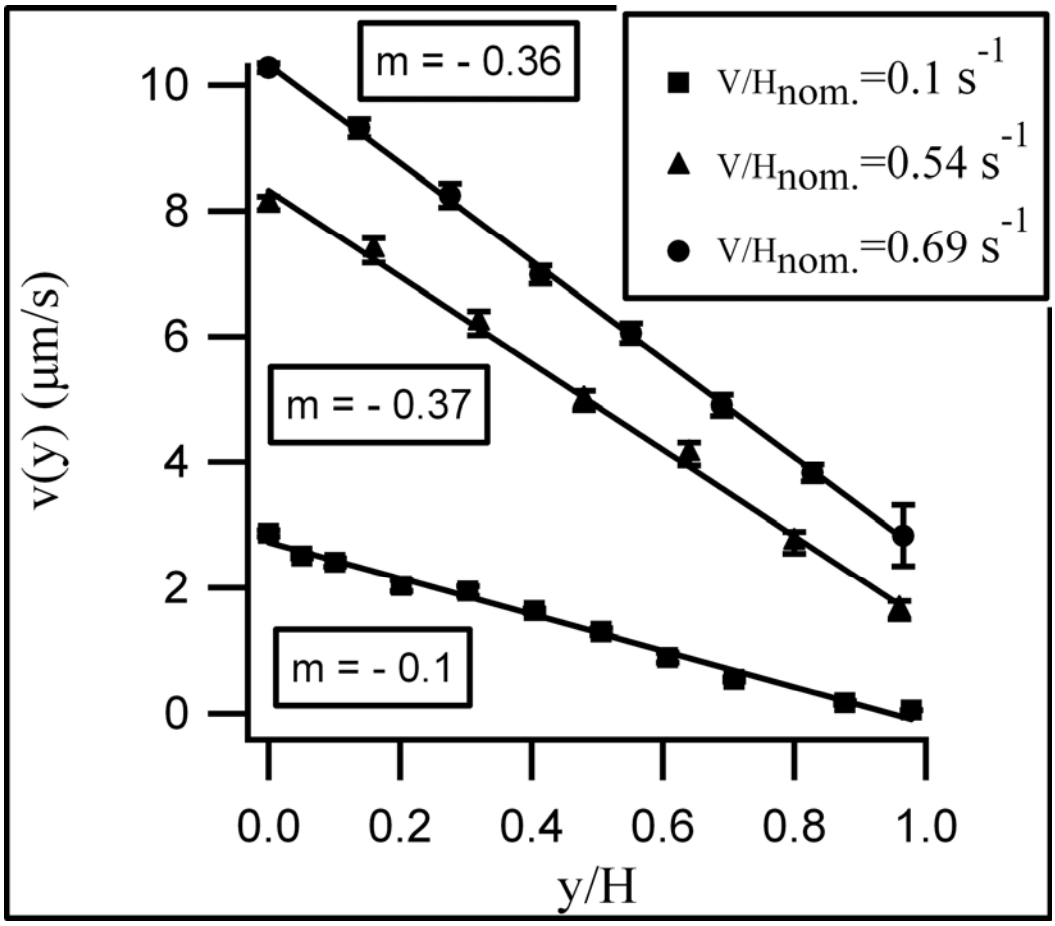

Figure 3.2: Velocity profiles for PBD200K, $\phi = 0.4$, Z = 32; y/H=0 and 1 are the bottom & top plates, respectively.

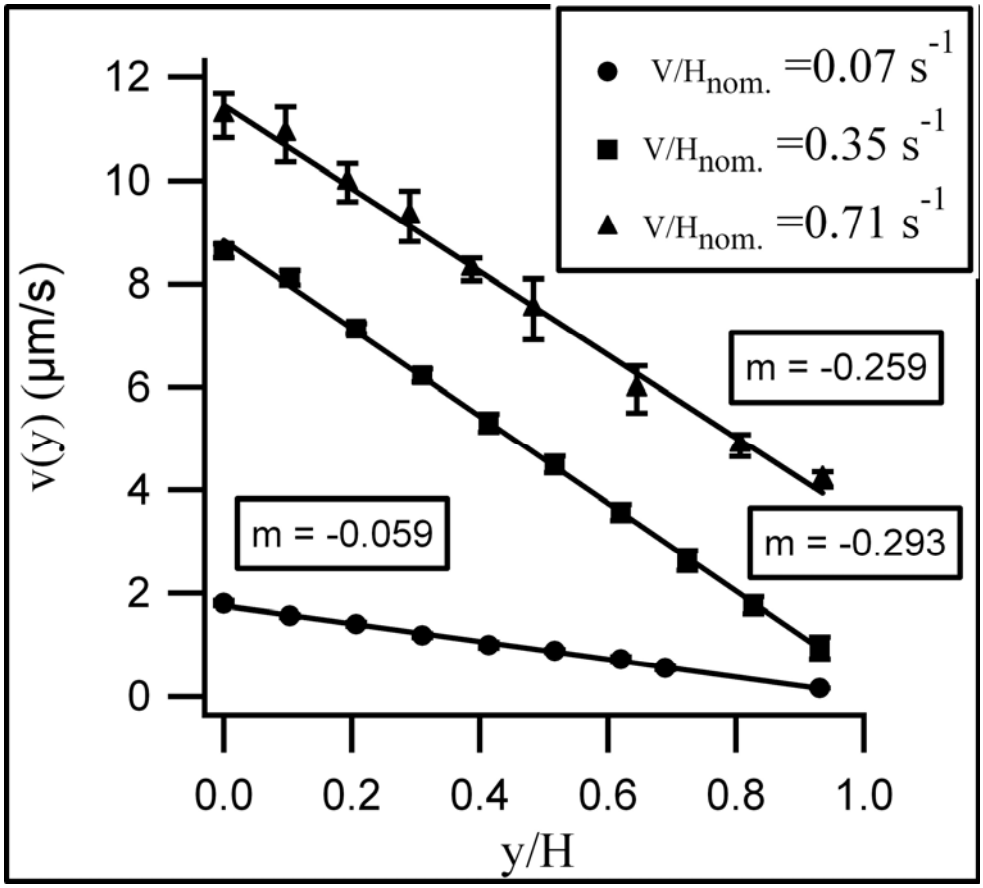

Figure 3.3: Velocity profiles for PBD200K, ϕ = 0.6, Z = 56; y/H=0 and 1 are the bottom & top plates, respectively.

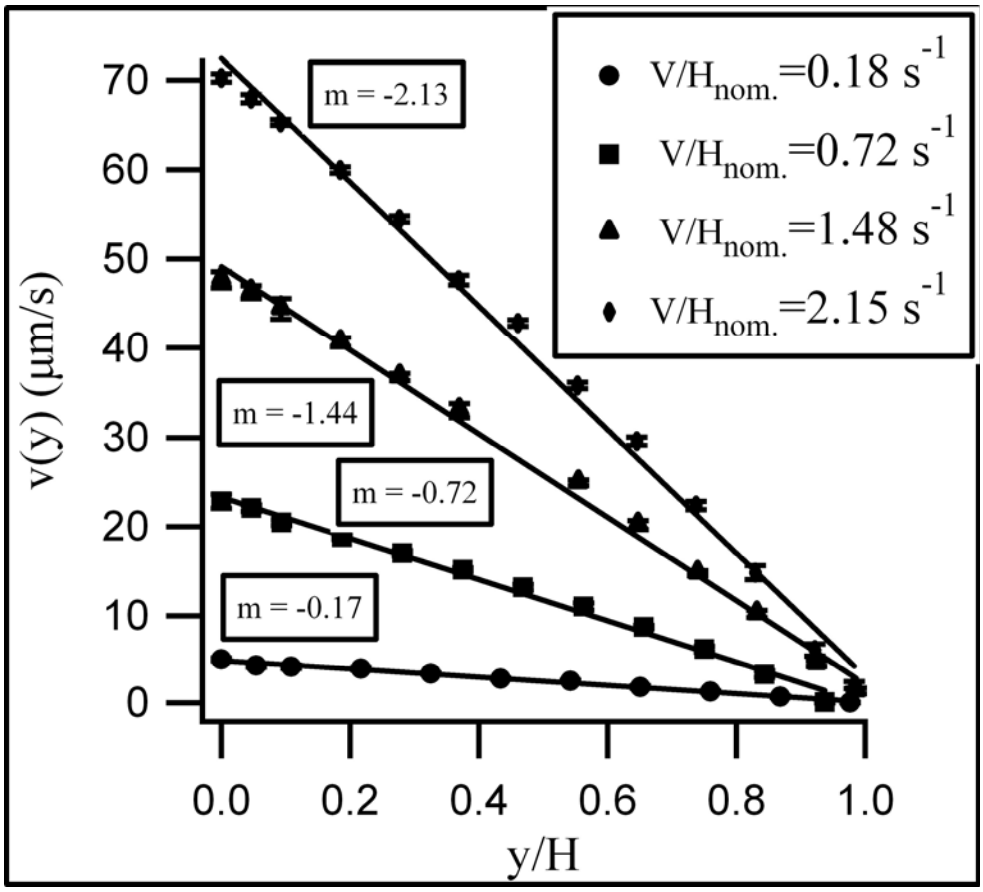

Figure 3.4: Velocity profiles for PBD788K, ϕ = 0.05, Z = 8; y/H=0 and 1 are the bottom & top plates, respectively.

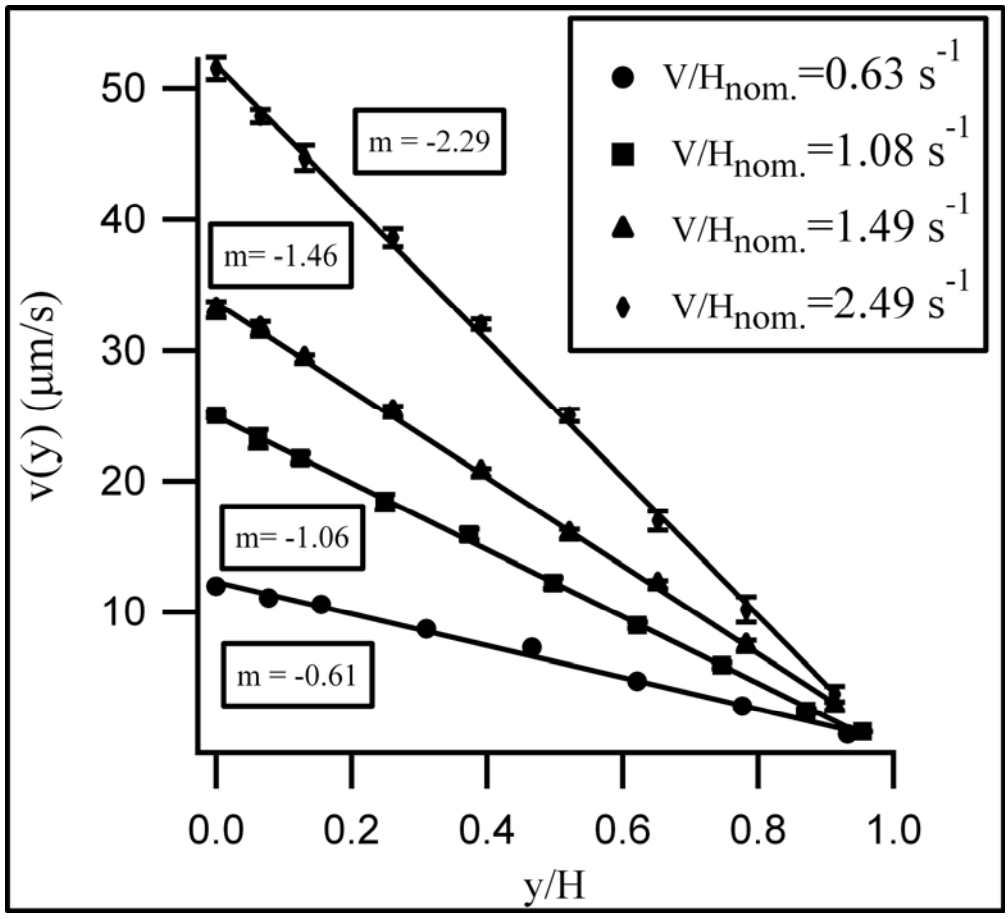

Figure 3.5: Velocity profiles for PBD788K, ϕ = 0.1, Z = 20; y/H=0 and 1 are the bottom & top plates, respectively.

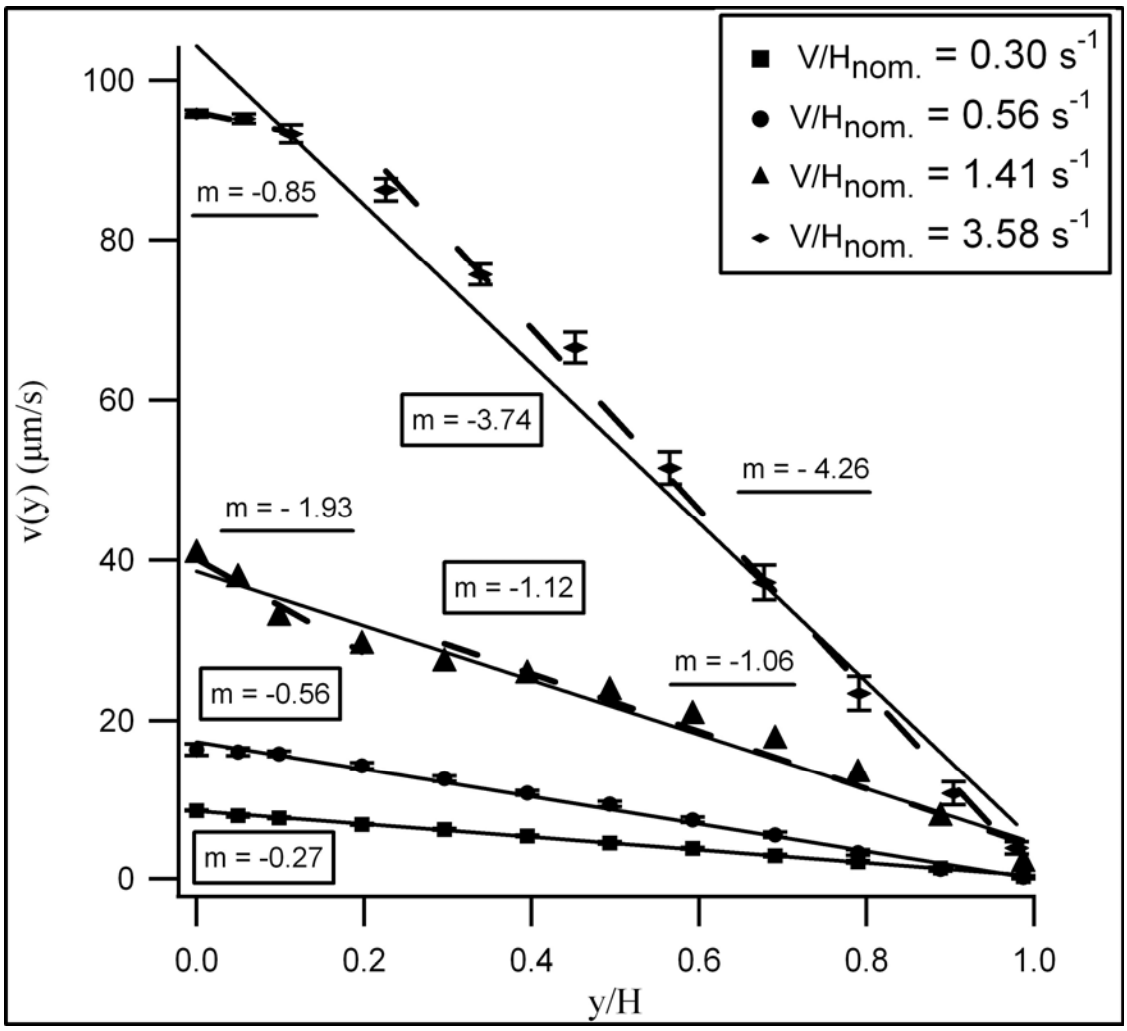

Figure 3.6: Velocity profiles for PBD788K, ϕ = 0.2, Z = 51; y/H=0 and 1 are the bottom & top plates, respectively.

The nominal and true shear rates are generally in excellent accord at low rates, $\dot{\gamma}_{nom.} << \tau_{rept}^{-1}$. Except for the most viscous solutions, $\dot{\gamma}_T \approx \dot{\gamma}_{nom}$ over the entire range of shear rates studied; for the PBD200K, $\dot{\gamma}_T$ becomes systematically lower than $\dot{\gamma}_{nom}$ with increasing shear rate. If the polymers are assumed to violate the no-slip condition equally at the two planes, the difference can be related to the *slippage velocity,* V_s: $\dot{\gamma}_{nom.} - \dot{\gamma}_T = 2\frac{V_s}{H}$. Figure 3.7 plots V_s against σ_s for two PBD 200K solutions - both manifest two well-defined slip regimes. At stresses below a critical value $\sigma_s^* / G_N \approx 1.97$ and 1.3, respectively, V_s is an approximately linear function of σ_s. At higher σ_s, slip violations are much larger and V_s increases rapidly. These observations are in good to excellent agreement with previous reports of interfacial slip in entangled polymers [21], based on other measurement techniques. Scaling theories [21-23] predict that slip by shear-induced disentanglement of surface-tethered and bulk polymer chains exhibit multiple power-law regimes in V_s versus σ_s, including the linear "Navier" slip regime observed here. These theories also predict a transition to large (macroscopic) slip velocities at $\sigma_s^* / G_N \approx 1$, which is also consistent with our experiments. Thus, we conclude that the stress plateau and erratic behavior seen in PBD200K solutions are not produced by bands, but by slip.

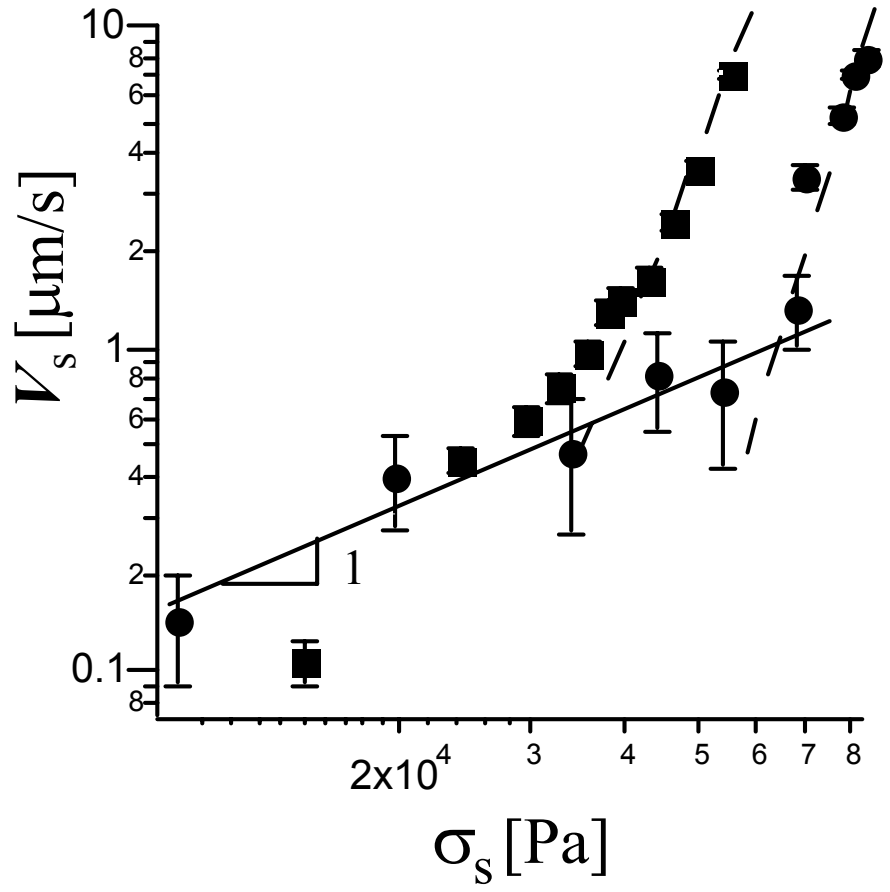

Figure 3.7: Slip velocity versus shear stress for PBD200K solutions, $Z = 32$ (squares), $Z = 56$ (circles).

Figure 3.6 provides velocity profiles for a more entangled version of the PBD788K polymer - Z = 51. Rheology measurements indicate that σ_s versus $\dot{\gamma}$ is monotonic in the range where banding is predicted. Figure 3.6 shows that at shear rates up to $\dot{\gamma}\tau_d = 18; \dot{\gamma}\tau_{rouse} \approx 0.12$, the velocity profile for this material is linear, with slope *m* close to the imposed shear rate, $(V/H)_{nom}$. At $\dot{\gamma}\tau_d = 45; \dot{\gamma}\tau_{rouse} = 0.3$, *m* begins to deviate from $(V/H)_{nom}$ and the velocity profile is weakly non-linear in the near-wall region. In this case, a single straight line with $m < (V/H)_{nom}$ still fits the data, but the fit is poorer near the moving boundary; a combination of two lines yields a shear rate near the moving boundary roughly twice that in the bulk fluid. A similar result is observed for the highest shear rate studied ($\dot{\gamma}\tau_d = 113; \dot{\gamma}\tau_{rouse} = 0.74$), with the apparent shear rate in the bulk now about 19% larger than $(V/H)_{nom}$.

It could be argued that the profiles for PBD788K, Z = 51 are consistent with banding; however, the unusually large rates, $\dot{\gamma}\tau_d \approx Z$, at which the deviations from linearity are first seen rule out any straightforward explanation by DE theory. Indeed at such high shear rates, chain stretching and normal stress effects are appreciable, making it impossible to ignore secondary flows, even in our carefully constructed shear device. Finally, considering the range of *Z*, solution viscosities, and dimensionless shear rates for which decidedly linear velocity profiles are observed, we conclude that shear banding is not a general feature of entangled polymer flows.

3.5 Conclusion

In conclusion, velocity profiles for entangled polymers in planar-Couette shear flow have been measured on the micron scale by combining confocal microscopy and velocimetry. Our results show that these profiles are generally linear for polymers with degrees of entanglement in the range 8 to 56, and inconsistent with the notion that shear banding is a characteristic of entangled polymer flows. Our results also show that entangled polymer solutions violate the no-slip condition and that at shear stresses comparable to the elastic modulus, highly nonlinear slip behavior (*strong-slip*) occurs.

Acknowledgements: This study was supported by the National Science Foundation (DMR0551185 and DMR0606040) and by KAUST-CU Center for Energy and Sustainability. We are grateful to Erik Herz and Prof. Ulrich Wiesner for providing fluorescent nanoparticle tracers used in the study.

REFERENCES

1) P.G. De Gennes, J. Chem. Phys. **55**, 572 (1971).
2) M. Doi and S. F. Edwards, *The Theory of Polymer Dynamics* (Oxford, New York, 1986).
3) K. Osaki, Rheol. Acta **32**, 429 (1993).
4) E.V. Menezes and W.W. Graessley, J. Polym Sci., Polym Phys Ed. **20**, 1817 (1982)
5) S. Baek, J. J. Magda and R.G. Larson, J. Rheol (N.Y.) **37**, 1201 (1993).
6) D.S. Pearson, Rubber. Chem. & Tech. **60,** 439 (1987)
7) J. Yerushalmi, S. Katz, and R. Shinnar, Chem. Eng. Sci. **25,** 1891 (1970).
8) G. Marrucci and N. Grizzuti, Gazz. Chim. Ital. **118**, 179 (1988).
9) N.A. Spenley, M.E. Cates, and T.C.B. McLeish, Phys. Rev. Lett. **71,** 939 (1993).
10) M. Britton and P. Callaghan, Phys. Rev. Lett. **78**, 4930 (1997).
11) M. R. López-González *et al*., Phys. Rev. Lett. **93**, 268302 (2004).
12) G. Marrucci, J. Non-Newt. Fluid Mech. **62**, 279 (1996).
13) G. Ianniruberto and G. Marrucci, J. Rheol. **45**, 1305 (2001); J. Non-Newt. Fluid Mech. **102**, 383 (2002).
14) D. W. Mead, R. G. Larson, and M. Doi, Macromolecules **31**, 7895 (1998).
15) J. Bent *et al.*, Science **301,** 1691 (2003).
16) S. T. Milner, T. C. B. McLeish, and A. E. Likhtman, J. Rheol. (N.Y.) **45**, 539 (2001).
17) R.S. Graham, A.E. Likhtman and T.C.B. McLeish, J. Rheol. (N.Y.) **47**, 1171 (2003).

18) V.R. Mhetar and L.A. Archer, J. Polym Sci. B **38**, 222 (2000); J. Non-Newtonian Fluid. Mech. **81**, 71 (1999).

19) F. Brochard-Wyart and P.G. deGennes, Langmuir **8**, 3033 (1992).

20) A. Ajdari *et al*., Physica (Amsterdam) **104A**, 17 (1994).

21) V. R. Mhetar and L. A. Archer, Macromolecules **31**, 6639 (1998); 8607 (1998).

22) Y. M. Joshi, A. K. Lele, and R.A. Mashelkar, Macromolecules **34**, 3412 (2001).

23) P. Tapadia, and S. Q. Wang, Phys. Rev. Lett. **96**, 016001 (2006).

24) P. Tapadia, S. Ravindranath, and S.Q. Wang, Phys. Rev. Lett. **96**, 196001 (2006).

25) P.E. Boukany and S. Q. Wang, J. Rheol. (N.Y.) **51**, 217 (2007).

26) Y.T. Hu and L. Wilen, J. Rheol. (N.Y.) **51**, 275 (2007).

27) I. Cohen *et al.*, Phys. Rev. Lett. **97**, 215502 (2006).

28) R.G. Larson, Rheol. Acta **31**, 213 (1992).

29) S. Kumar and R.G. Larson, J. Non-Newtonian Fluid Mech. **95**, 295 (2000)

30) Y.W. Inn, K. F. Wissbrun, and M. M. Denn, Macromolecules **38**, 9385 (2005)

31) C. Sui and G.B. McKenna, Rheol. Acta **46**, 877 (2007)

32) V. R. Mhetar and L.A. Archer, J. Rheol. (N.Y.) **40**, 549 (1996)

33) R. B. Bird, R.C. Armstrong, and O. Hassager, *Dynamics of Polymeric Liquids* (Wiley, New York, 1987), Vol. 1.

CHAPTER 4

The Constitutive Curve and Velocity Profile in Entangled Polymers during Start-up of Steady Shear Flow

4.1 Summary

Transient constitutive curves and transient velocity profiles of entangled polymers in steady shear flow were obtained from rheometry and confocal microscopy respectively. The shear stress, σ (t) is measured from start-up to steady state at discrete times over a wide range of shear rates. Both constant-time and constant-strain transient constitutive curves: $\sigma(\dot{\gamma})$ *vs.* $\dot{\gamma}$ can be constructed from these measurements. On short time scales, the transient curves were often multi-valued in shear stress; this condition improves as steady-state is approached. The transient curves are then compared to the steady-state constitutive curve and to the velocity profiles, which were also measured at distinct times on the way to steady state. The velocity profile data was obtained by combining confocal microscopy and particle image velocimetry (PIV) in a custom-built shear cell with plate separation, H: $0.075 \leq H \leq 0.43$ mm. We studied polybutadiene and polystyrene solutions seeded with fluorescent 150nm silica and 7.5 μm melamine particles. Our results give insight into how interfacial slip develops with time and also yield information about molecular relaxation dynamics.

4.2 Introduction

Recent velocity profile measurements using micron-sized particles dispersed in entangled polybutadiene solutions show, for the first time, that steady shear flow of entangled polymer liquids is unstable to shear banding at moderate and high shear rates [1-3]. An important feature of these studies is that shear banding occurs even in moderately entangled polymer solutions, generally thought to be well-described by tube model constitutive theories amended to include mechanisms like convective constraint release [4-8] and Rouse relaxation of chain length [9]. Parameters such as shear strain and shear rate, widely used to characterize shear flow of entangled polymers, are ill-defined in a banded fluid. The presence of bands in these fluids therefore raises obvious questions about the reliability of decades-worth of nonlinear rheological data obtained in these systems.

In a previous article [10], we pointed out that confocal microscopy measurements can be used to recover the velocity profile in entangled polymers in a setting free of the secondary flow and edge effects that normally plague shear flow experiments of highly elastic polymers. Specifically, we used spatially resolved displacement measurements of nanometer-sized, fluorescent tracers dispersed in entangled polymers. These polymers were under shear flow in a narrow-gap (H = 25-35 μm), high-aspect ratio (W/H > 142), planar Couette shear cell. In this study, the steady-state velocity profiles were obtained for polymer solutions covering a range of molecular weights and degrees of entanglement ($8 \leq Z \leq 56$). Our experiments showed that the steady-state velocity profile in all moderately entangled, and some well-entangled polymer solutions are straight lines with slopes essentially equal to the applied shear rate, even at rates well into the non-Newtonian shear flow regime ($\dot{\gamma} \gg \tau_d^{-1}$). This finding is inconsistent with expectations for a shear-banded fluid.

For the remaining well-entangled polymer solutions, linear velocity profiles were also observed, but the slopes were found to diverge markedly from the imposed shear rate, even at rates $\dot{\gamma} < \tau_d^{-1}$, i.e. before the onset of the non-Newtonian regime. In reference 10, this feature was analyzed by assuming that the solutions slip uniformly at the shear cell surfaces, and this analysis yielded slip velocity versus shear stress profiles in agreement with earlier reports [11]. On this basis, it was concluded that when artifacts due to interfacial slip are avoided, the steady-shear velocity profile in entangled polymer solutions is inconsistent with the notion that shear-banding is a universal characteristic of these materials.

A perhaps obvious concern about this conclusion is that the phenomena analyzed as interfacial slip, could well reflect the onset of bands, with the steepest bands localized within microscopic regions near both shear cell surfaces. This argument linking apparent slip violations in an entangled polymer to strong gradients in the velocity profile produced by non-monotonic shear stresses in the bulk liquid is clearly not new [12]. It is also compatible with the recent particle velocimetry measurements in entangled polybutadiene solutions reported by Ravindranath and Wang [13], in which interfacial slip usually preceded observations of shear banding.

An arguably more intriguing explanation of our earlier results comes from recent theoretical studies of Adams and Olmsted [14], which show that "shear-banding-like" behavior can be observed even for entangled polymers with a monotonic constitutive curve at steady state. Specifically, these authors solved the equation of motion for an entangled polymer in shear flow using a version of the Rolie-Poly (RP) model [15], which was modified to include a stress "diffusion" term [16-17] to describe the fluid's response to an inhomogeneous viscoelastic stress. Results from this analysis reveal a phenomenon, we here term "apparent shear banding", which originates from spatial

gradients in velocity and shear stress in curvilinear flow geometries. The phenomenon is expected to vanish at steady-state in a planar-Couette shear geometry, but could result in pronounced transient shear-bands in highly entangled polymer liquids when convective-constraint release and sub-Rouse, transient chain stretching effects are ignored.

In the current study, we extend our earlier confocal rheometry technique to characterize the velocity profiles in entangled polymers under large-gap conditions, designed to minimize interfacial slip effects [18]. Motivated by the recent analysis of Adams and Olmsted [14], we also characterize the time-dependent evolution of the flow curve and velocity profiles in entangled polymer liquids during start-up of steady shear flow. An unexpected benefit of the former experiment is that the transient flow curve measurements provide insight into both the fluid-scale and molecular-scale transient response to steady shear flow.

4.3 Materials and Experiment

Entangled polystyrene and polybutadiene solutions (Table 1) were used in all experiments reported. To characterize the velocity profile in these materials, they were seeded either with nano-sized (diameter ~ 150nm), fluorescent, core-shell, silica tracer particles, known as C dots [in narrow-gap studies] or with 7.5 μm spherical, melamine particles incorporating fluorescein isothiocyanate (FITC) (Corpuscular Inc.) [in large-gap studies]. C dots encapsulating a tetramethylrhodamine fluorophore in their core (kindly provided by Prof. Ulrich Wiesner, MS&E Dept., Cornell) were synthesized using a variant of a previously published routine [19-21]. To maximize dispersion in

the polymer solution, the C dots were first surface modified with n-hexadecyltrichlorosilane and dispersed in a tetrahydrofuran (THF) carrier solvent.

To create fluorescent polymer solutions, a selected polymer melt and a chemically identical oligomer or diethyl phthalate solvent, were added in the desired proportions in a large amount of THF co-solvent. The resultant solution was combined with the Cdot/THF or melamine/THF solution and mixed thoroughly using a magnetic stirrer. The THF co-solvent was subsequently evaporated at room temperature, and the last traces driven off in a vacuum oven.

Table 4.1: Properties of polymer solutions used in the study

Sample	***Z***	***τ_d (s)***	***$G_N x10^{-4}$ (Pa)***	***$\eta_0 x10^{-5}$ (Pa-s)***
PBD 200K, φ=0.6 Solvent: 5K PBD	56	0.92	46	2.7
PS 8.42M, φ=0.06 Solvent: DEP	11	12.7	0.048	0.12

Details of the confocal rheology measurement device (Figure 4.1) and procedure used to recover the velocity profile have been reported previously [10]. In the current study, the time-dependent velocity profiles in polymer solutions with a range of entanglement densities ($11 < Z < 51$) were characterized using narrow gap ($H \approx 75\mu m$) and large-gap ($H \approx 230\text{-}430\mu m$), planar Couette shear flow measurements. A perhaps obvious disadvantage of the large-gap experiments is that the sample aspect ratio is large, which makes the measurements, particularly at high shear rates $\dot{\gamma} \geq \tau_d^{-1}$, susceptible to artifacts produced by secondary flow [22]. To reduce this effect, the area of the top plate was increased from 5 mm^2 (narrow-gap experiments) to 7 mm^2 (large gap experiments), yielding aspect ratios ($a_s = W/H$) ≥ 14.

In addition to the obvious advantage of reducing the influence of wall slip on the velocity profile, the larger gaps allow for concomitantly larger tracers, which allow measurements to be performed at lower magnification (10 X). This feature is advantageous because it allows tracers to be measured in a wider field of view, which provides a more effective method for interrogating possible secondary flows in the solutions. To ascertain that, at all the particle sizes used, the seeded particles function exclusively as tracers, small-amplitude oscillatory shear measurements were performed in identical samples, with and without particles. This verified that flow was unaffected by the presence of the particles.

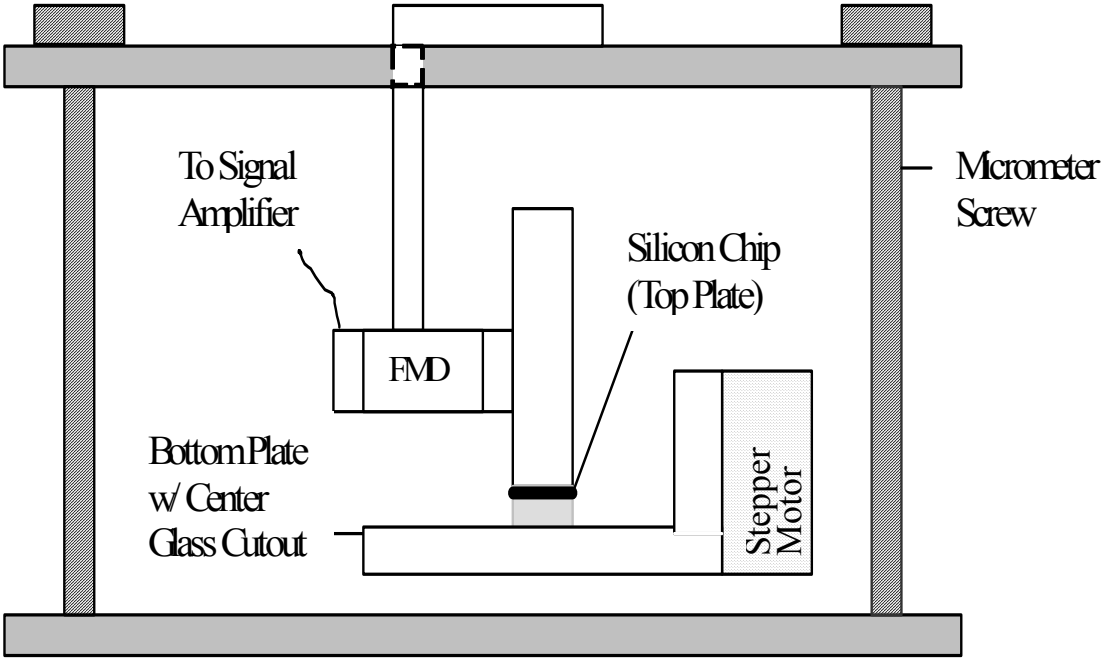

Figure 4.1: Schematic (Front View) of Shear Cell

To characterize the velocity profile during shear flow, MATPIV was used to measure the particle speed in different layers throughout the planar-Couette cell gap. A force measurement device (FMD) [10], attached to the top shearing surface, was used to simultaneously measure the shear force during start-up of steady shear. The FMD is connected to a signal conditioning amplifier. In the calibration procedure, different loads were applied to the top plate and the corresponding change in voltage (ΔV) is recorded. $\sigma = F^{*}\text{Area}^{\text{plate}}$ and in the resultant calibration curve, $F = k(\Delta V)$; k = constant.

By synchronizing the time intervals at which the velocity profile was recorded with the changes in the transient shear force, we were able to measure velocity profiles at intervals covering the full range of stress regimes (i.e. from start-up: t = 0 to steady state. $t = t_{ss}$ - defined here as the time required for the shear force to reach a plateau) (See Figure 4.2).

As a complement to the planar-Couette shear measurements, steady shear rheology experiments were performed using a Rheometric Scientific (ARES) rheometer outfitted with cone and plate fixtures: CP10-5.4° and CP25-5. An important benefit of these experiments is that they allow the constitutive curves, $\sigma(\dot{\gamma})$ vs $\dot{\gamma}$, to be determined as a function of time or shear strain over the same range of shear rates and for the same materials investigated using the planar-Couette shear flow device. It is understood that although the confocal technique allows us to determine velocity profiles in the fluid at multiple discrete times, and as such might be thought to directly reflect the instantaneous $\sigma(\dot{\gamma})$ vs $\dot{\gamma}$ profile, in even a moderately elastic material, these profile are also dependent on the local stress history. A qualitative connection between the measured velocity profiles and constitutive curves obtained at discrete shear strains might therefore prove beneficial.

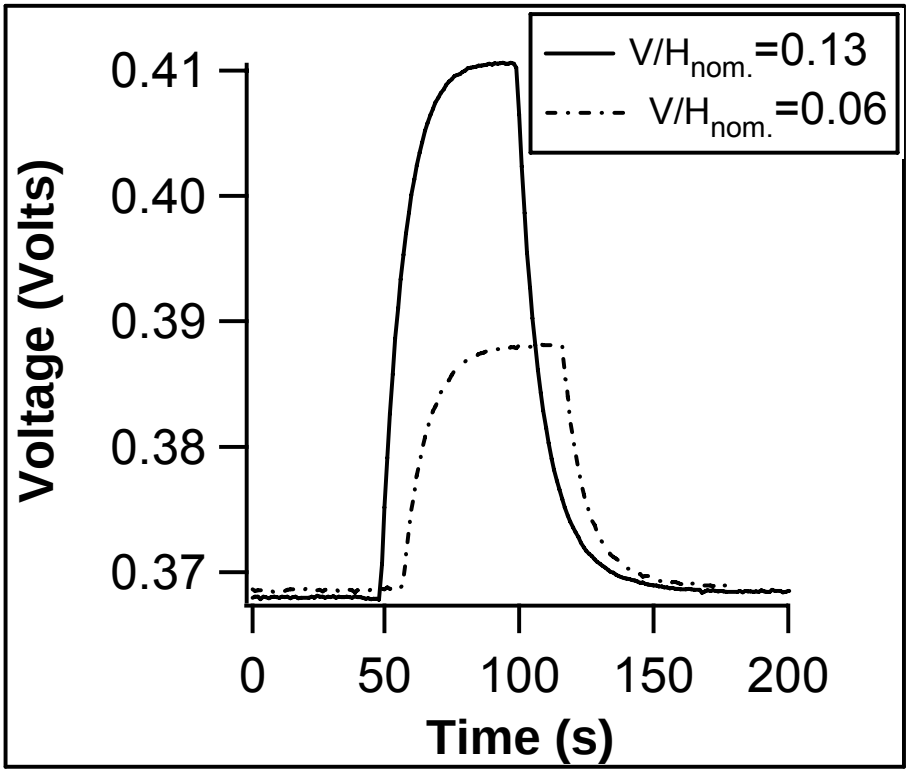

Figure 4.2: Typical FMD result during shear start-up in confocal rheology experiment

4.4 Results and Discussion

Figure 4.3 reports the instantaneous constitutive curves σ / G_e vs $Wi_d \equiv \tau_d \dot{\gamma}_d$ for a well-entangled polybutadiene solution (PBD200K60%, Z = 56) obtained by dissolving a 1,4-polybutadiene melt: $\bar{M}_w = 2\text{x}10^5\ g/mol$, $\bar{M}_w / \bar{M}_n = 1.05$, (PBD200K, synthesized in-house) in a weakly entangled PBD oligomer host, $\bar{M}_w = 5\text{x}10^3\ g/mol$. The plateau modulus, G_e, used to non-dimensionalize the shear stress was obtained from oscillatory shear measurements in the linear viscoelastic (LVE) regime, from which G_e is determined as the storage modulus value that corresponds to the loss minimum in the plateau regime. The characteristic relaxation time, τ_d was also determined from LVE experiments; it is defined here as the reciprocal of the oscillatory shear frequency, ω, at which the imaginary part of the complex viscosity, $\eta''(\omega) \equiv G'(\omega)/\omega$, manifests a global maximum, i.e. just prior to the terminal regime. The solid line in Figure 4.3 is the constitutive curve, $\sigma(Wi_d) = G^*(\omega\tau_d)$, obtained by enforcing the Cox-Merz rule.

Figure 4.3 shows that, at the earliest times, $\sigma(\dot{\gamma}) = b\dot{\gamma}$, implying that the initial flow curve is Newtonian at all shear rates. However, when the effective viscosity, κ, is calculated from the slope, b, of these early-time transient curves, the κ values ($1.6\text{x}10^4 \le \kappa \le 2.8\text{x}10^4\ Pa \cdot s$) are at least an order of magnitude smaller than the zero-shear viscosity, η_0 (see Table 4.1). It is straightforward to show that the linear relationship between shear stress and shear rate can also be expressed in the form: $\sigma(\dot{\gamma}) = (tG_e)\dot{\gamma}$, where t is the time following start-up of shear at t = 0 and G_e is the elastic modulus of the polymer. This relationship therefore implies that $\kappa \approx tG_e$, hence the initial linear $\sigma(\dot{\gamma})$ *vs.* $\dot{\gamma}$ relationship reflects an affine elastic response of the material to shear. When the κ values are compared to (tG_e) values for the two earliest times (t=0.6, 0.1), we find that the two values are in fact similar, as expected from an affine linear elastic response. Figure 4.4 shows that κ reaches a steady value at long

time and this steady-state κ ($2.3x10^5$) is comparable to the zero shear viscosity ($2.7x10^5$).

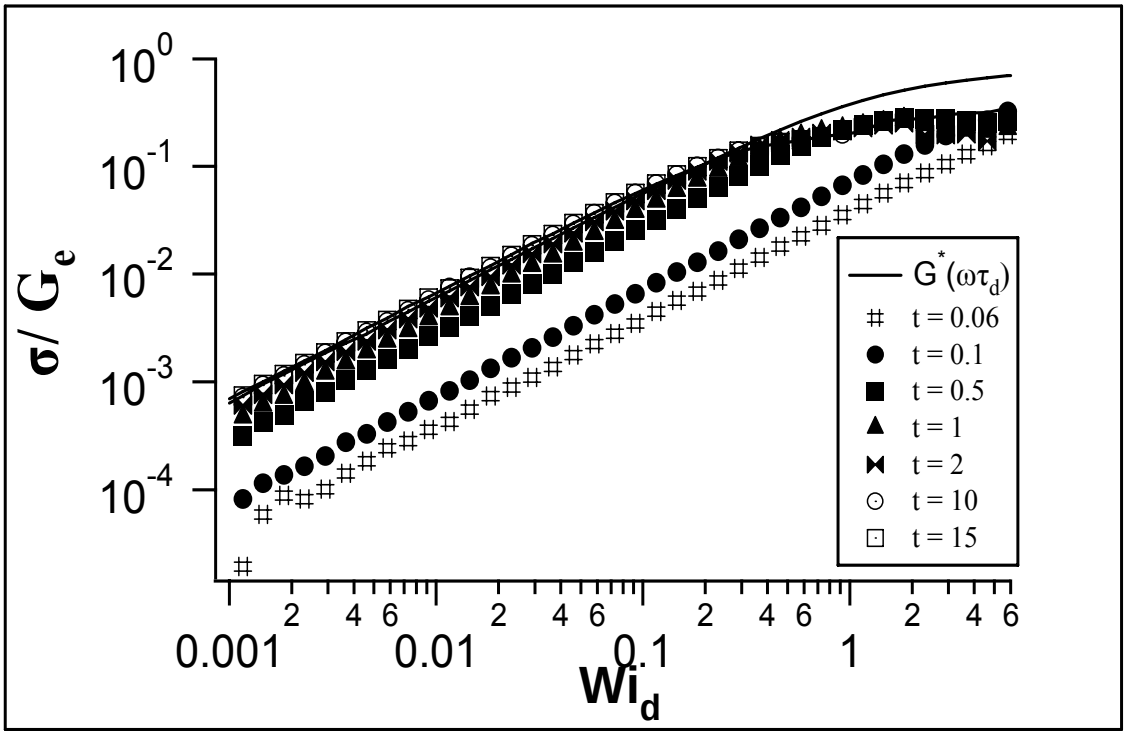

Figure 4.3: Constant-time, dimensionless transient Constitutive Curves for PBD 200K60%_5K

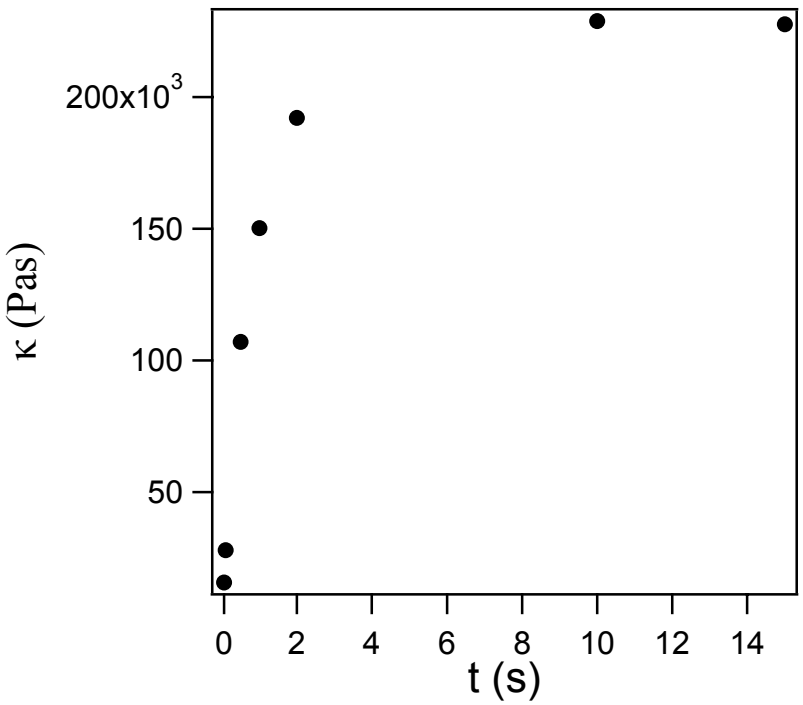

Figure 4.4: Effective viscosity (κ) vs. time for PBD 200K60%_5K; κ is calculated from the slope of the linear portion of the transient constitutive curves.

The linear relationship: $\sigma(\dot{\gamma}) = b\,\dot{\gamma}$ is observed to gradually disappear at shear rates $\dot{\gamma} \sim \tau_d^{-1}$, i.e. $Wi_d \sim 1$ and there is evidently a small plateau, in which shear stress is independent of time and shear rate, at the highest rates studied (Figure 4.3). This finding suggests that beyond a critical shear rate order $Wi_d \sim 1$, the stress ceases to be affected by the deformation conditions. This observation is a consequence of the arrested relaxation of oriented polymer chains, in flow on time scales of order the reptation time.

The constant-strain (Figure 4.5) curves for this same polymer show that for the smallest strains ($\gamma \leq 0.1$), there is a slope change in $\sigma(\dot{\gamma})$ at $\gamma \approx Wi_d$. This again reflects that an affine response gives way to a non-affine one when the molecular stain, $\dot{\gamma}\tau_d$, exceeds the value: $\dot{\gamma}t$. The non-affine regime therefore reflects the role of molecular relaxation. The open symbols in these curves ($\gamma \leq 0.251$) are stress data, σ (t), for times shorter than the calculated transducer compliance time, τ_T; $\tau_T^{calculated} =$ 0.099 for this polymer using: $\tau_T = 5\pi\eta_0 D^3 / 6\alpha K_T$. If these controversial points are excluded, there is still a flattening of the constant-strain, constitutive curves at the highest Wi_d values. Therefore multiple shear rates correspond to the shear stress plateau region, which could lead to distinct shear rate bands in the fluid. To further investigate this, we studied this polymer via confocal rheology.

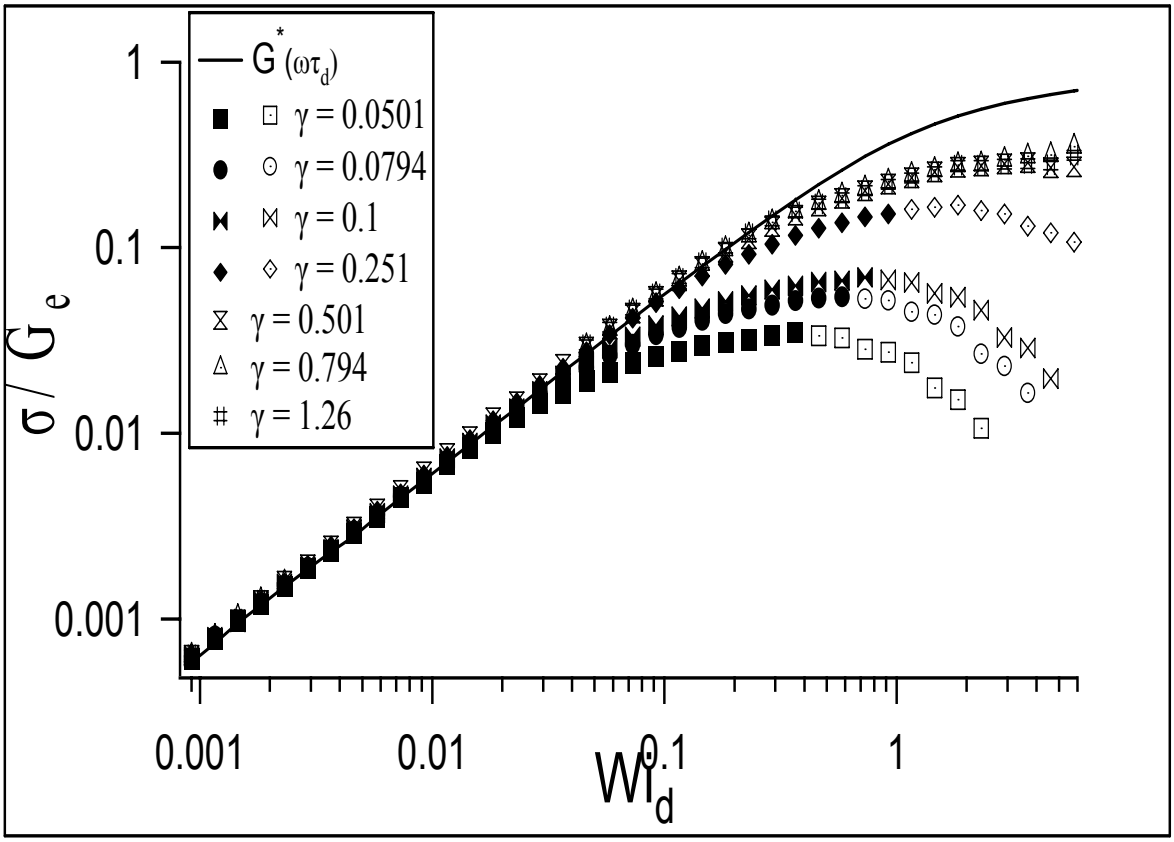

Figure 4.5: Constant-strain, dimensionless transient Constitutive Curves for PBD200K60%_5K

In PIV experiments with PBD200K60%, *H* was decreased by half; this gaps size is evidently large enough to control slip (Figure 4.6-a). All the transient profiles are linear (Figure 4.6-b). However, the transient slip velocities (Figure 4.6-c) show that V_s begins at a maximum, non-zero value then decreases to a negligible value within 2-3 seconds after imposition of steady shear. This trend of apparent early-time slip is only seen with this polymer and is likely due to device compliance errors. G_N is proportional to τ_T/τ_d, where τ_T is the transducer compliance time [24] and device compliance delays are minimized when $\tau_T/\tau_d \ll 1$. The plateau modulus of this solution is three orders of magnitude larger than G_N of PS8.42M6%, which might explain why this apparent early-slip is not seen in the latter (Figure 4.8). We also calculated the compliance, K, of our device using beam deformation equations [25] and find K ~ 10 μm/N.

(a)

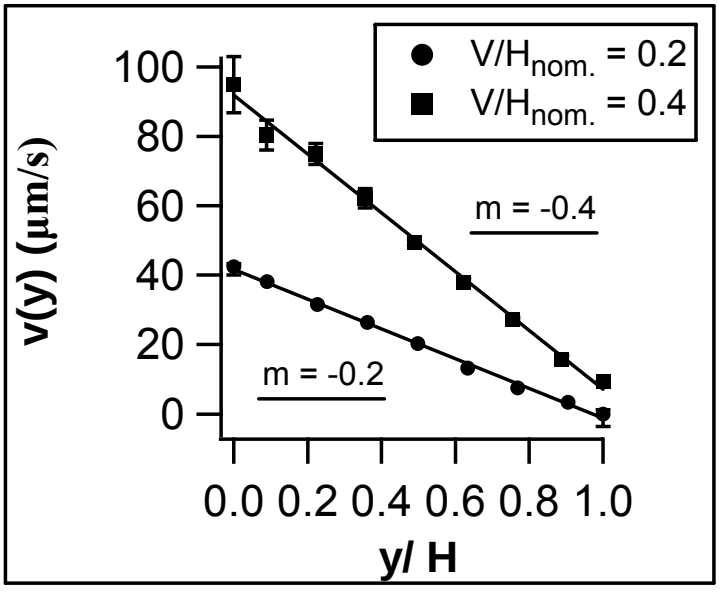

Figure 4.6-a: PBD200K60%_5K at H ~ 223 μm (a) Steady-state velocity profiles

(b)

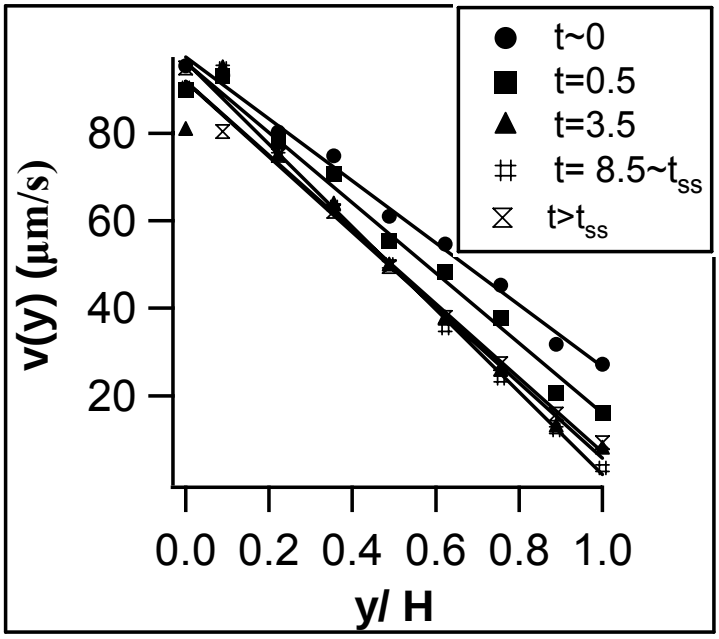

Figure 4.6-b: PBD200K60%_5K at H ~ 223 µm: Transient shear profiles; t=0 is start of shear

(c)

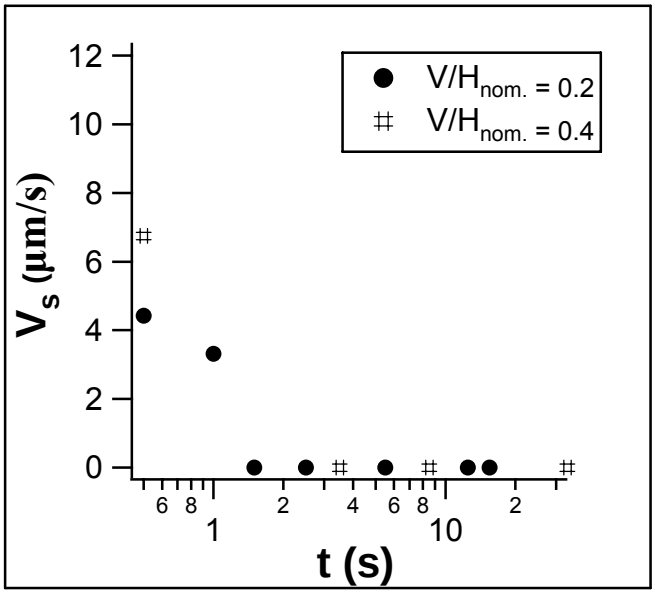

Figure 4.6-c: PBD200K60%_5K at H ~ 223 µm: Transient slip velocities; t=0 is start of shear

Similar constant-time, $\sigma(\dot{\gamma})\ vs.\ \dot{\gamma}$ measurements are performed for a moderately entangled polystyrene solution (Figure 4.7). For this experiment, $\tau_T^{calculated} = 0.1$ seconds. In this polymer, flow is also affine on the shortest time scales (t=0.1), then quickly transitions to non-affine curves. The constitutive curves are clearly multivalued on intermediate time scales (see t =1.0 and t = 2.51 in "blown-up" high shear rate region in Figure 4.7-b). These curves transition to monotonic relationships at a time slightly larger than 10 seconds, i.e. comparable to $\tau_d = 12.7$. We point out that Convective Constraint Release (CCR), the mechanism which removes the maximum in $\sigma^{ss}(\dot{\gamma})\ vs.\ \dot{\gamma}$ should become important precisely on these time scales, implying that CCR stabilizes the flow at steady state.

(a)

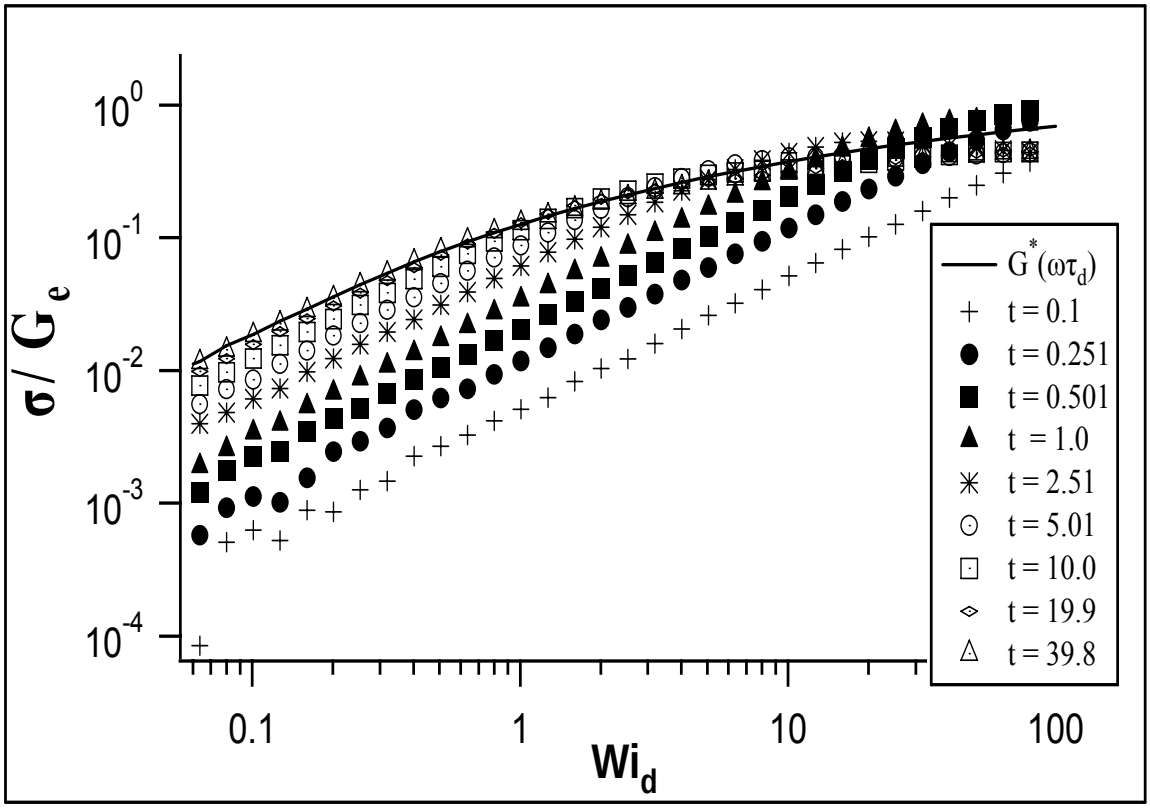

Figure 4.7: Constant-time, dimensionless transient Constitutive Curves for PS8.42M6%

Figure 4.7 continued

(b)

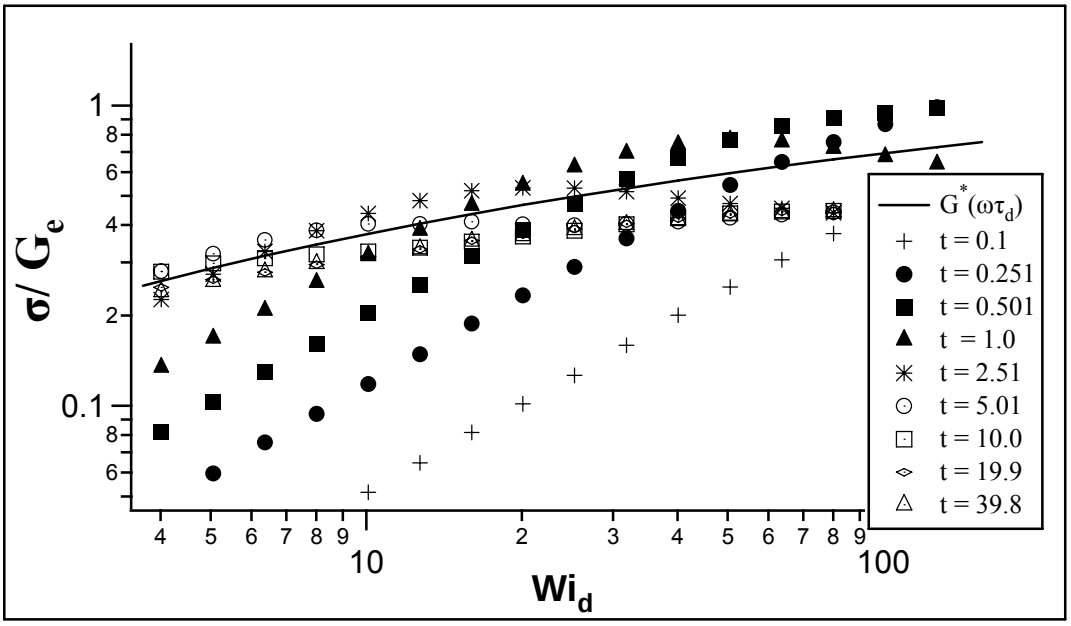

Transient PIV experiments will illuminate any signs of unstable flow in the fluid's velocity profile at intermediate times. Also since the τ_d of this polymer is larger, we can probe shear rates that are further into the non-Newtonian shear regime. In the planar-Couette shear cell with H=75 μm, there is evidence of slip even at relatively low shear rates i.e. V/H_{true}, which is the slope of the measured velocity profile, differs from the applied shear rate, $V/H_{nom.}$ As shear rate increases so does the degree of slip: (V/H_{nom} - V/H_{true}). And at $\dot{\gamma}=0.08$ which corresponds to $\dot{\gamma}\tau_d = 1$, the D-E threshold for the start of shear banding, there is a significant amount of slip but the profile is not banded (Figure 4.8-a).

We compare this shear profile data to that for $\dot{\gamma}_{nom.}$, which is more than twice as large and for a plate separation that is nearly six times larger. Interestingly we find that under the larger shear rate conditions where both interfacial slip and shear banding might be expected to become worse, there is no evidence of either (Figure 4.8-b).

Therefore, increasing the gap size can eliminate (or greatly minimize) interfacial slip leading to a more controlled shear environment. If slip is no longer the dominant mechanism, we should be able to detect shear banding, if it exists. The fact that we observe linear profiles is consistent with the idea that shear banding does not occur in entangled polymers. Moreover, it supports our earlier conclusion that the shear rate discrepancy between the imposed and measured shear rates for H = 75 μm is caused by interfacial slip. Slip is inversely proportion to gap size, H, as $\dot{\gamma}_{nom.} / \dot{\gamma}_T = 1 + 2b / H$ where b is the slip length.

(a)

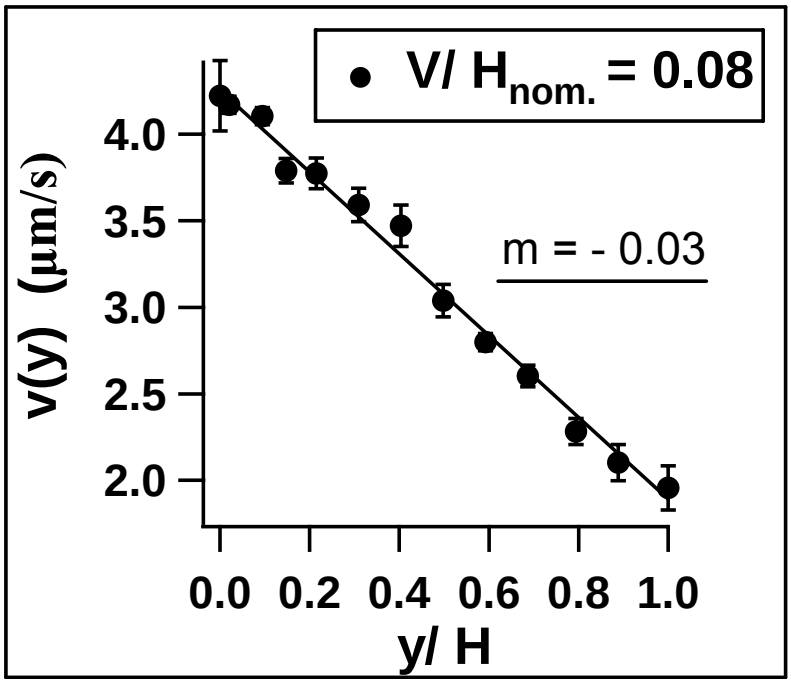

Figure 4.8: Velocity profiles for PS 8.42M6% at (a) H = 75 μm and (b) H= 425 μm

Figure 4.8 continued

(b)

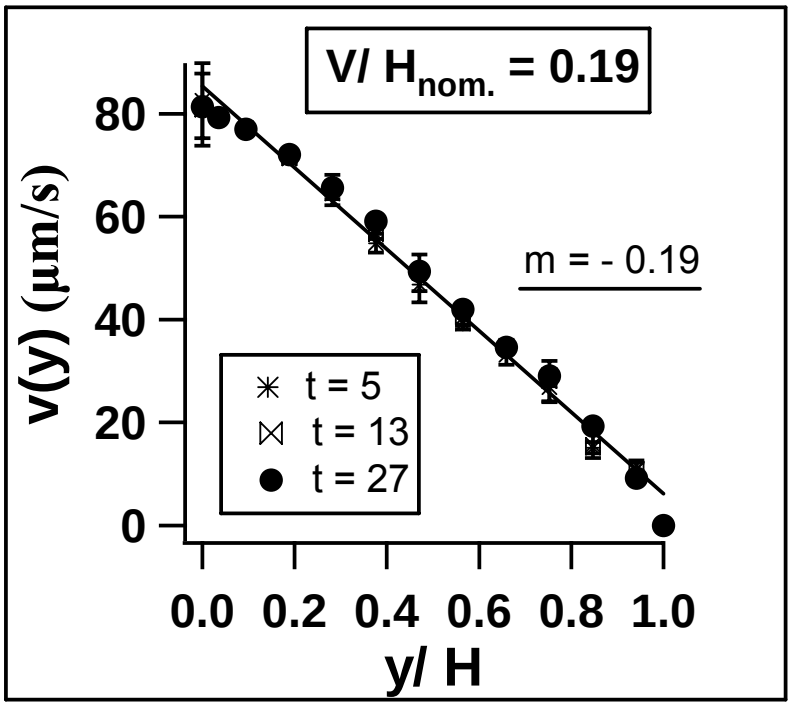

As for the PBD200K60% solution, all the transient shear profiles for the PS solution are linear (Figure 4.9) for both shear cell gaps studied. The transient profiles at the larger gap (H = 425 μm) show no evidence of slip in contrast to the narrow gap transients. For $V/H_{nom} = 0.081$, the profile was measured at eight different one-second intervals on the way to steady state.

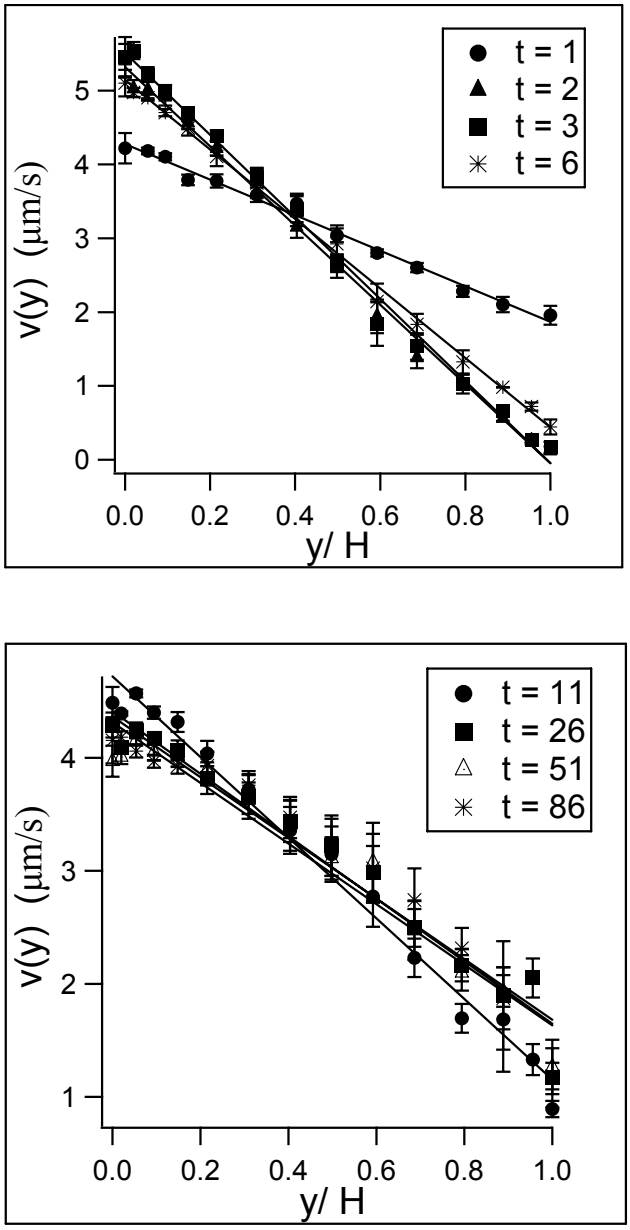

Figure 4.9: Transient profiles for PS8.42M6%, $V/H_{nom.} = 0.081$, H = 75 µm

Figure 4.10 summarizes the slip velocity, V_s: $\dot{\gamma}_{nom.} - \dot{\gamma}_T = 2\frac{V_s}{H}$ calculated from each profile. Slip is initially negligible (cf. early affine response in transient rheometry data) but grows as the shear duration increases, eventually reaching an approximately constant value.

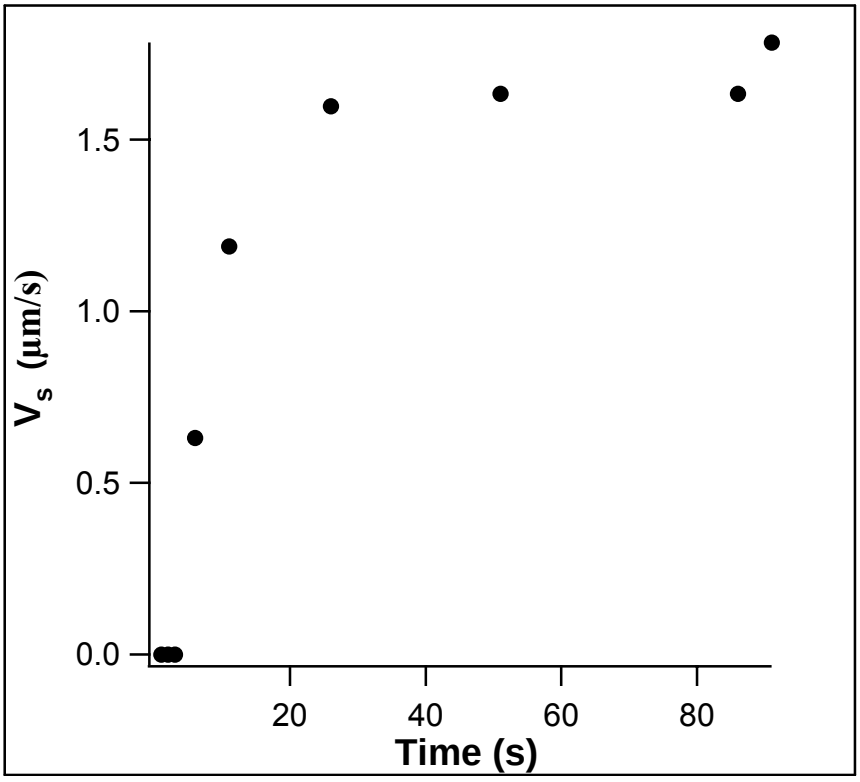

Figure 4.10: Slip velocity from transient profiles for PS8.42M6%, $V/H_{nom.}$ = 0.081, H = 75 μm

It is somewhat surprising that the transient non-monotinicity in Figure 4.7 first appears at $Wi_d \approx 10$. According to the D-E Theory this behavior should first begin at $Wi_d \approx 1$. To understand the molecular mechanism that might be occurring during the start-up of steady shear experiments, we model the polymer's flow response. A variant of the Islam-Archer (IA) differential constitutive model [26] with CCR incorporated into the original model, is used to study transient behavior (Figures 4.11 and 4.12) of a model polymer ($Z=20$, $\tau_d = 1$ and $G_N = 1$).

First we note that at the shortest times, the response is affine just as in our experiments (Figures 4.3 & 4.7). We compare constant-time $\sigma(\dot{\gamma})$ *vs.* $\dot{\gamma}$ curves with CCR switched on and off. If relaxation via CCR is not allowed to occur (Figure 4.12), the intermediate-time, multi-valued curves persist and even the steady state curve is multi-valued. Conversely, the polymer recovers from this intermediate, unstable state if CCR is turned on. This result provides direct evidence of the role played by CCR in stabilizing shear flow of entangled polymers.

From the full set of results presented in this chapter, it is tempting to conclude that while transient constitutive curves in an entangled polymer are more unstable than those at steady state, there is other missing physics that appears to stabilize shear flows. Hence linear velocity profiles can be measured even in situations where the transient flow curves are non-monotonic and therefore unstable.

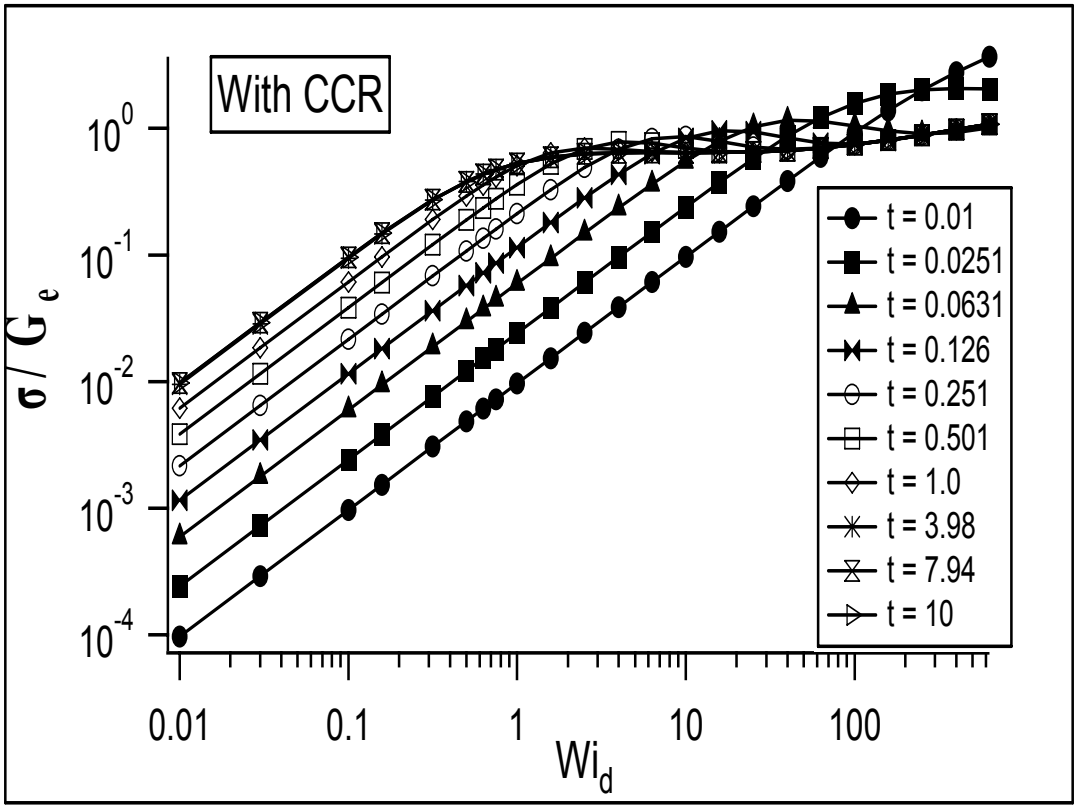

Figure 4.11: Constant-time, dimensionless, transient Constitutive Curves for model polymer, with CCR included

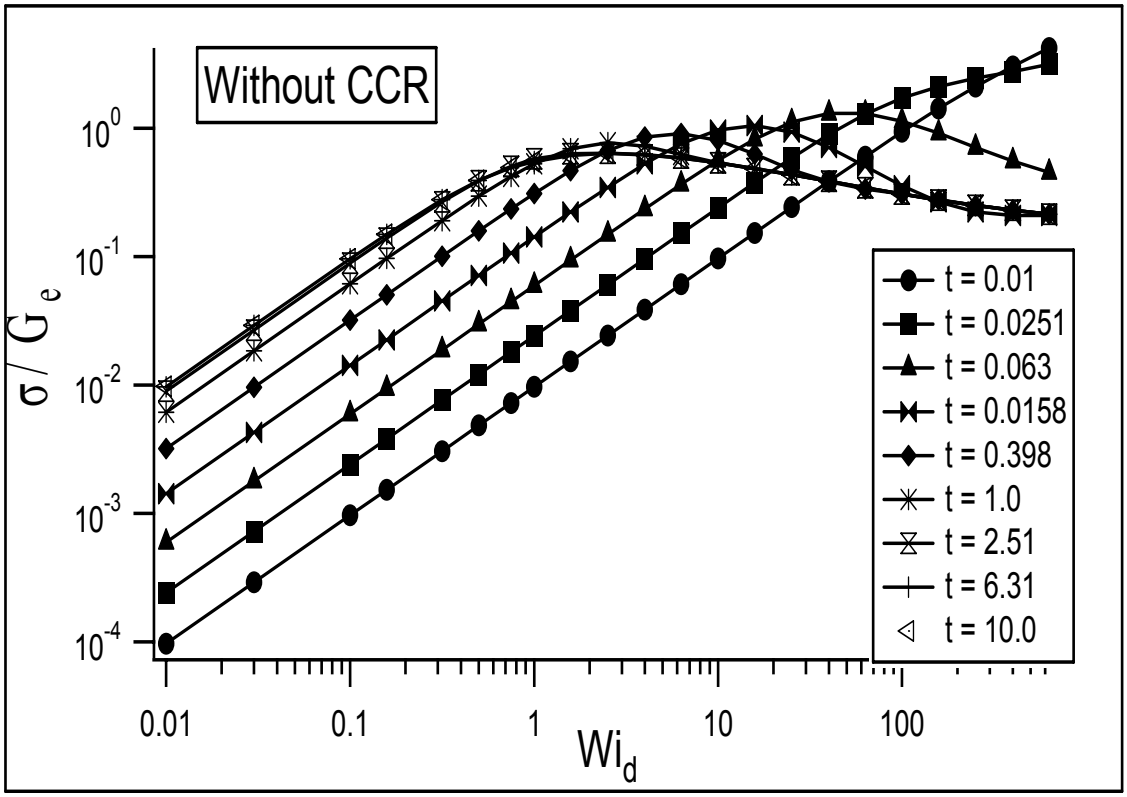

Figure 4.12: Constant-time, dimensionless, transient Constitutive Curves for model polymer, without CCR

4.5 Conclusion

By complementing narrow-gap confocal rheology (confocal microscopy and PIV) with similar experiments at macroscopic dimensions, we find that one can reduce interfacial slip to negligible levels through using sufficiently large gaps. In this more controlled setting, entangled polymer solutions do not shear band, as predicted by D-E Theory (for $\dot{\gamma}\tau_d > 1$). Recent arguments that shear banding exists at transient times are not supported by our confocal rheology data. In all cases, the transient profiles are linear. Under conditions (small H, higher shear rates) where the profile does show steady-state interfacial slip, this is preceded by "transient" slip, which steadily increases before reaching a steady level.

For the same shear rate range, constant-time and constant-strain transient constitutive curves are qualitatively similar. Only one of the polymer solutions (the least entangled) displayed characteristics of shear banding in transient constitutive curve measurements. Moreover, this propensity to shear band was not detected in transient velocity profile measurements via confocal rheology. Both experimental and modeling results suggest that the stabilization of shear flow is due to the start of CCR as an additional relaxation mechanism for reducing stress.

REFERENCES

1) P. Tapadia, and S. Q. Wang, Phys. Rev. Lett. **96,** 016001 (2006).
2) P. Tapadia, S. Ravindranath, and S.Q. Wang, Phys. Rev. Lett. **96**, 196001 (2006).
3) P.E. Boukany and S. Q. Wang, J. Rheol. **51**, 217 (2007).
4) **G.** Ianniruberto and G. Marrucci, J. Rheol. **45**, 1305 (2001); J. Non-Newtonian Fluid Mech. **102**, 383 (2002).
5) S.T. Milner, T. C. B. McLeish, and A. E. Likhtman, J. Rheol. **45**, 539 (2001).
6) R.S. Graham, A.E. Likhtman and D. W. Mead, R. G. Larson, and M. Doi, Macromolecules **31**, 7895 (1998).
7) J. Bent et al, Science **301,** 1691 (2003).
8) R.S. Graham, A.E. Likhtman and T.C.B. McLeish, J. Rheol. **47**, 1171 (2003).
9) T. C. B. McLeish and R.C. BALL, J. Polym. Sci. Polym. Phys. Ed. **24** (1986) 1735; T.C.B. McLeish, J. Polym. Sci., Polym. Phys. Ed. **25**, 2253 (1987).
10) K. A. Hayes, M. R. Buckley, I. Cohen and L. A. Archer, Phys. Rev. Lett. **101**, 218301 (2008).
11) V.R. Mhetar and L.A. Archer, Macromolecules **31**, 6639 (1998); 8607 (1998).
12) M.E Cates, T.C.B. McLeish and G. Marrucci, Europhys. Lett. **21**, 451 (1993).
13) S. Ravindranath and S. Q. Wang, J. Rheol. **52**, 957 (2008).
14) J. M. Adams and P. Olmsted, Phys. Rev. Lett. **102**, 067801 (2009).
15) A. E. Likhtman and R. S. Graham, J. Non-Newtonian Fluid Mech. **114**, 1 (2003).
16) P.D. Olmsted, O. Radulescu, C.-Y.D. Lu, J. Rheol. **44**, 257 (2000).
17) J. M. Adams, S. M. Fielding, and P. D. Olmsted, J. Non-Newtonian Fluid Mech. **151**, 101 (2008).

18) J. Sanchez-Reyes and L. A. Archer, Langmuir **19,** 3304 (2003).

19) H. Ow, D. R. Larson et al Nano Lett. **5**, 113 **(**2005).

20) A. Burns, H. Ow, and U. Wiesner, Chemical Society Reviews **35***,* 1028 (2006).

21) E. Herz, A. Burns et al., Proceedings of SPIE, 6096 (2006).

22) V.R. Mhetar and L.A. Archer, J. Rheol. **40**, 549 (1996).

23) Y.W. Inn, K. F. Wissbrun and M. M. Denn, Macromolecules **38,** 9385 **(2005).**

24) C.S. Dutcher and D.C. Venerus, J. Non-Newtonian Fluid Mech. **150**, 154 (2008).

25) M. Ashby and D. Jones, *Engineering Material: An Introduction to their Properties and Applications* (Pergamon Press, Oxford, 1980).

26) M.T. Islam and L. A. Archer, J. of Polym. Sci., Part B: Polym. Phys. **39**, 2275 (2001).

CHAPTER 5

Linear and Nonlinear Viscoelastic Behavior of Entangled Star Polymer Solutions And Unentangled Star Polymer Melts

5.1 Summary

In part I of a two-part star polymer rheology study, we used step shear experiments to characterize the damping functions, h(γ), of weak to moderately entangled solutions (0.2≤φ≤0.8) of a symmetric 3-arm star polyisoprene: M_n^{arm} = 101K. We found that the $h(\gamma) \equiv G(t \geq \tau_k, \gamma) / G(t, \gamma \to 0)$ data lies on a single damping function curve for all entangled star-branched polyisoprene solutions. This "universal" damping function is more strain-softening than the D-E prediction. In part II, we studied the linear viscoelastic properties of unentangled, 4-arm, symmetric, star-branched polystyrene melts (0.47 K ≤ M_n^{arm} ≤ 4K). Linear viscoelastic data shows Rouse-like characteristics such as proportional relationships for η (M_n) and T_g (1/ M_n). And in step shear flow in these polymers, we are able to measure the Rouse model prediction: h (γ) = 1.

5.2 Introduction

A persistent topic of interest in polymer rheology is the range of pertinence of the successful Doi and Edwards (D-E) Theory [1]. There is extensive work showing that the theory fails in predicting stress relaxation after step shear flow of highly entangled polymers [2-6], where it is expected to work best. Other data suggests that the original theory is inadequate in predicting nonlinear flow behavior of polymers that are only weakly entangled and polymers, which have non-linear architectures [4, 7-10]. Limited data exists on linear viscoelasticty of branched polymers with unentangled arms [11-12], and there is even less experimental work on nonlinear rheology of theses systems. This paper presents results in this area for unentangled (short-arm), symmetric stars.

"Tube" [13] models for branched polymers incorporate relaxation mechanisms like "thermally activated" arm retraction [14] and dynamic dilution [15], which assumes that faster relaxing portions dilute the entanglement network by releasing constraints on unrelaxed portions. Milner & McLeish [14] developed a parameter-free theory for describing stress relaxation of star polymer melts. In their model, which includes dynamic dilution and higher Rouse modes for diffusive arm retraction over short distances, the only adjustable parameters are the entanglement molecular weight, N_e and the monomer friction coefficient, ξ. The model agrees well with linear viscoelastic data for stars of different chemistry (different N_e and ξ).

More recently, Lee et al. [16, 17] proposed a model for predicting linear viscoelasticty of branched melts and entangled star-branched polymer solutions by building upon Frischknecht et al.'s tube model [18]. In Lee et al.'s mechanism, which is based on hierarchical relaxation (arms first then backbone), the tube diffusion coefficient of the backbone is an explicit function of the number of short arm

entanglements. This self-consistent theory was successfully extended to polymer solutions by scaling the model parameters: M_e, τ_e and G_N, to their θ-solvent values (e.g. $G_N(\varphi_p) = G_N\varphi^{7/3}$).

In step shear flow: $\gamma = \gamma_0 H(t)$, The Doi-Edwards prediction for the damping function (with the independent alignment approximation) is: $h_{DE}(\gamma) = (1+0.18*\gamma^2)^{-1}$. The experimental damping function (valid for $t > \lambda_k$, the time-strain factorability time) is: $h_{exp}(\gamma) = G(t, \gamma)/ G(t, \gamma \rightarrow 0)$. Early publications by Vrentas and Graessley [2] and Osaki et al [19] show good correlation between the unmodified D-E theory and step shear data for entangled star-branched polymers. But, in the decades that followed, non-D-E damping was reported by various groups [4, 8-10] leading to nonlinear rheology modeling [20] for branched polymers.

To date, there is no reliable, universal model for nonlinear rheology of all branched polymers. Our goal in this paper is to complement the wealth of data [9, 11-12, 21-22] on linear viscoelasticity of branched polymers with step shear data for well-characterized stars with varying levels of entanglement, including unentangled arms. We also compare our results to the D-E model.

5.3 Materials and Experiment

Short arm, symmetric polystyrene stars (R) and a symmetric 1, 4-polyisoprene star (S) were synthesized "in house" using anionic polymerization under high vacuum conditions. Synthesis details and molecular weight characterization for these polymers has been previously published [16-17]. Extensive linear viscoelastic property characterization was done for the 1, 4-polyisoprene star (S) solutions [23] used in our study. The properties of all the polymers are shown in Tables 5.1 & 5.2. The

molecular weight between entanglements, M_e, for polystyrene and polyisoprene is 17, 000 g/mol and 4200 [17] g/mol respectively [$M_e(\varphi_p) = M_e/\varphi^{4/3}$].

Step shear and small-amplitude oscillatory shear experiments were performed with an Anton Paar Physica modular, compact rheometer (MCR 300) outfitted with a variety of stainless steel, cone and plate: CP10-5, CP4-4, CP8-1 and parallel plate: PP4 fixtures. Stress relaxation experiments were done at 28 ºC for all the polyisoprene (S) solutions and at 25 ºC above the glass transition temperature, T_g, of the star (R) polystyrenes. For the polystyrenes, T_g is the maximum in G"(T) vs. T in dynamic temperature sweep experiments (Figure 5.1). The temperature range for the polystyrene measurements was 73-128 ºC.

Table 5.1: Properties of entangled polyisoprene star (S101K) solutions; solvent = 4K PI

φ	τ_k (s)	τ^d (s)	N/N_e	η_0 (Pas)
0.2	0.2	0.06	2	6.65×10^2
0.3	0.4	0.19	4	4.66×10^3
0.4	0.7	0.42	7	1.58×10^4
0.5	1.1	1.13	9	6.12×10^4
0.7	0.1	6.80	14	5.20×10^5
0.8	9.5	21.7	17	1.67×10^6

Table 5.2: Properties of 4-arm Polystyrene melts

Sample	M_n^{star} ***(kg/mol)***	T_g ***(°C)***	$\eta_0 x\ 10^{-8}$ ***(Pas)***
R30	16.8	101.2	4.48
R29	12.6	95.7	3.74
R28	7.4	86.3	2.37
R27	6.3	82.7	2.51
R26	4.8	77.2	1.85
R25	2	47.6	1.66

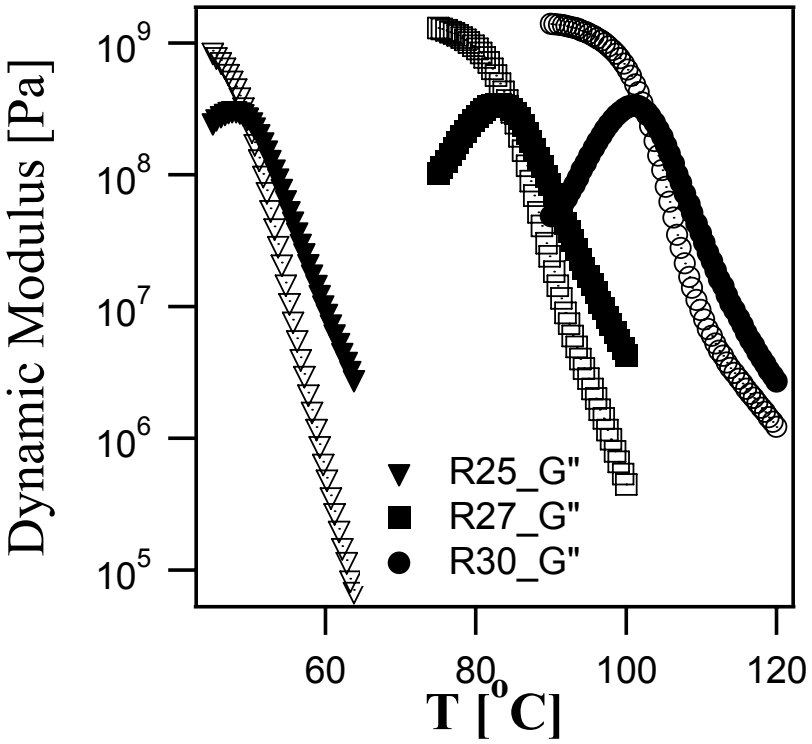

Figure 5.1: Dynamic temperature sweep data for unentangled polystyrene stars

5.4.1 Results and Discussion – Entangled Polyisoprene Star Solutions

Table 5.1 shows that the increasing concentration of short linear chains dilutes the effective entanglement network of the stars since there is a general trend for the factorability time (τ_k) to decrease with decreasing entanglement density. This observation is consistent with a slower arm retraction process in more entangled solutions. For star polymers, where reptation is not possible since one end of the chain is fixed to the branch point, arm retraction is an important relaxation mechanism. Longer, more entangled arms will take a longer time to completely relax stress by stretching and retracting down their respective tubes. We do note that $\varphi = 0.7$ appears to be anomalous in this general trend.

Figures 5.2 & 5.3 show the stress relaxation data for two of the polyisoprene solutions. The time scale for factorability is of order the longest relaxation time, τ_d – a result which has also been observed in linear entangled polymers [24, 25]. This is another discrepancy with the Doi-Edwards theory, which expects τ_k to be much closer to τ_{Rouse}.

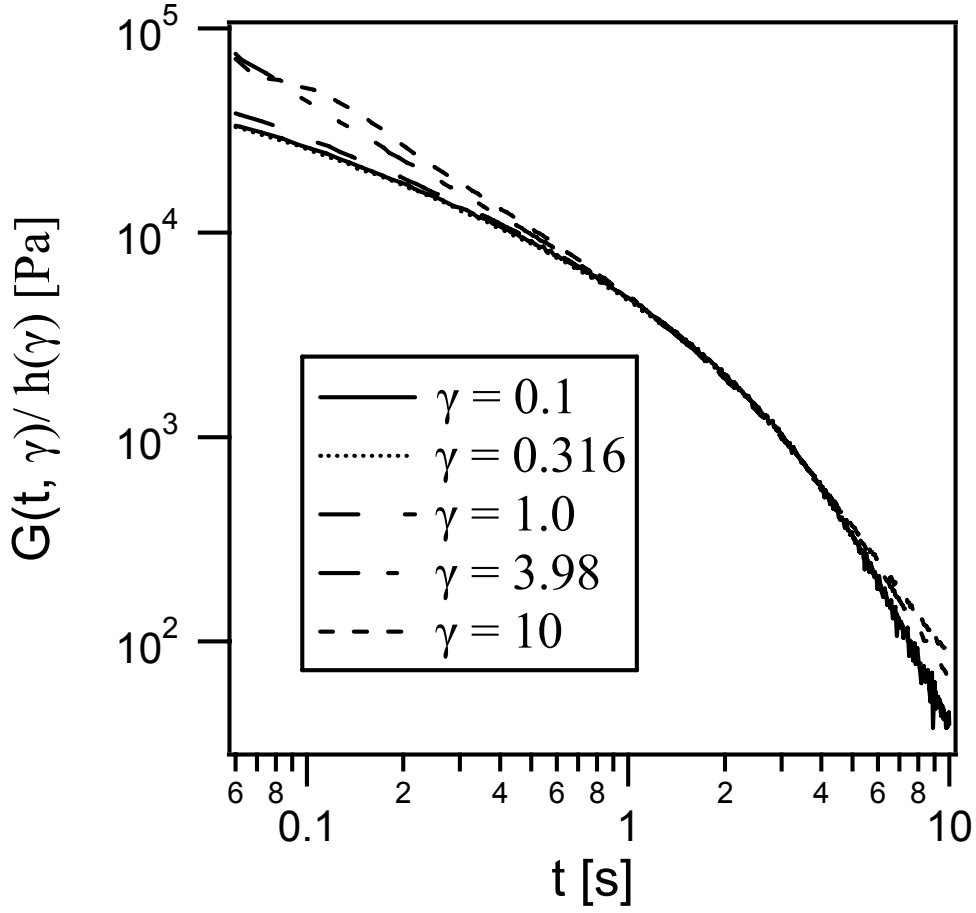

Figure 5.2: Shifted non-linear modulus G (t, γ) for PI Star: S101K, φ = 0.4

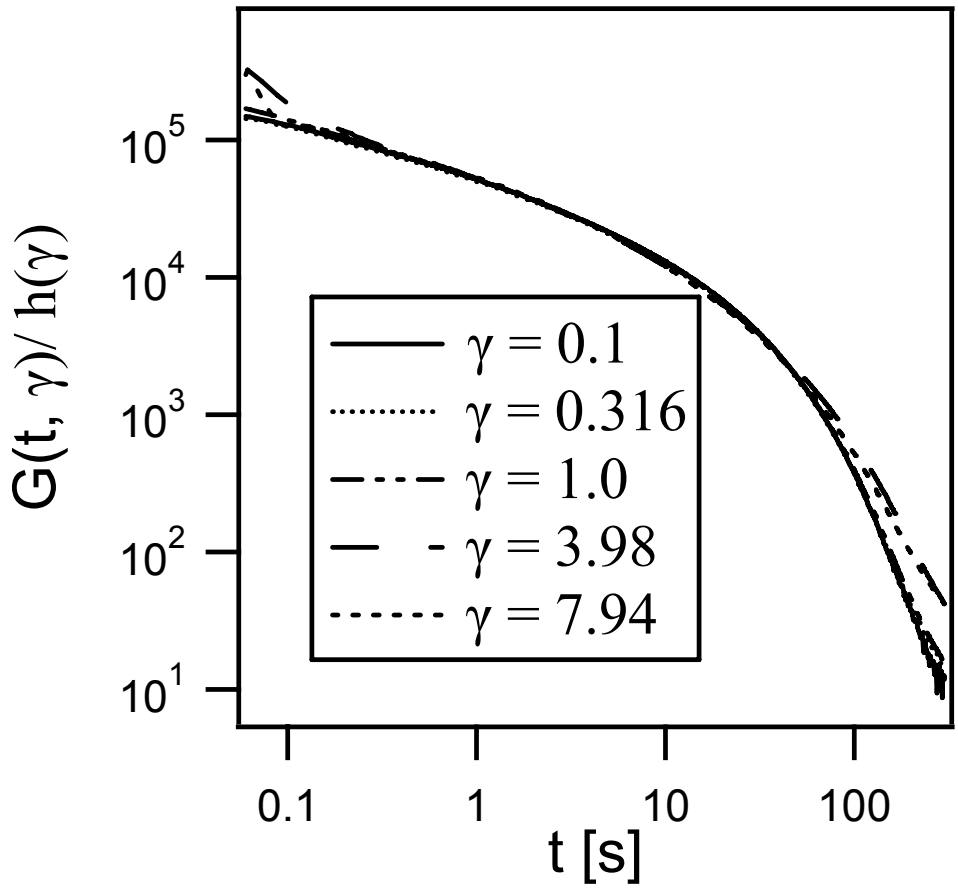

Figure 5.3: Shifted non-linear modulus G (t, γ) for PI Star: S101K, φ = 0.7

The damping function data is evaluated for $t > \lambda_k$ for all the solutions because for $t > \lambda_k$, $h_{exp}(\gamma)$ is independent of time. We find that the data can be fitted by a single curve (Figure 5.4) for all the S101K solutions ($2 \leq N^{arm}/ N_e \leq 17$). The equation: $h2 = (1+0.36*\gamma^2)^{-1}$has the same form as the DE-IA prediction; but, the strain pre-factor is twice that of $h_{DE-IA}(\gamma)$. Our results differ from Osaki's step shear results [19] with stars having similar number of entanglements. For star-branched polystyrenes ($10\leq N^{arm}/ N_e \leq 38$), this author found good agreement (even better than for linear polymers) between h_{D-E} and $h_{exp}(\gamma)$. Their result is a little surprising. Since one end of the star arm is tethered to a branch point, one would not expect its relaxation to follow a model based on deGennes' reptation concept.

In Figure 5.4, we see that there is no gradation in the damping function as solutions go from scarcely to moderately entangled, ruling out a simple Type C Damping explanation [4]. The fact that the 'quality' of the damping function is unaffected by varying the entanglement density suggests that the damping function might be unique and universal for all entangled star solutions.

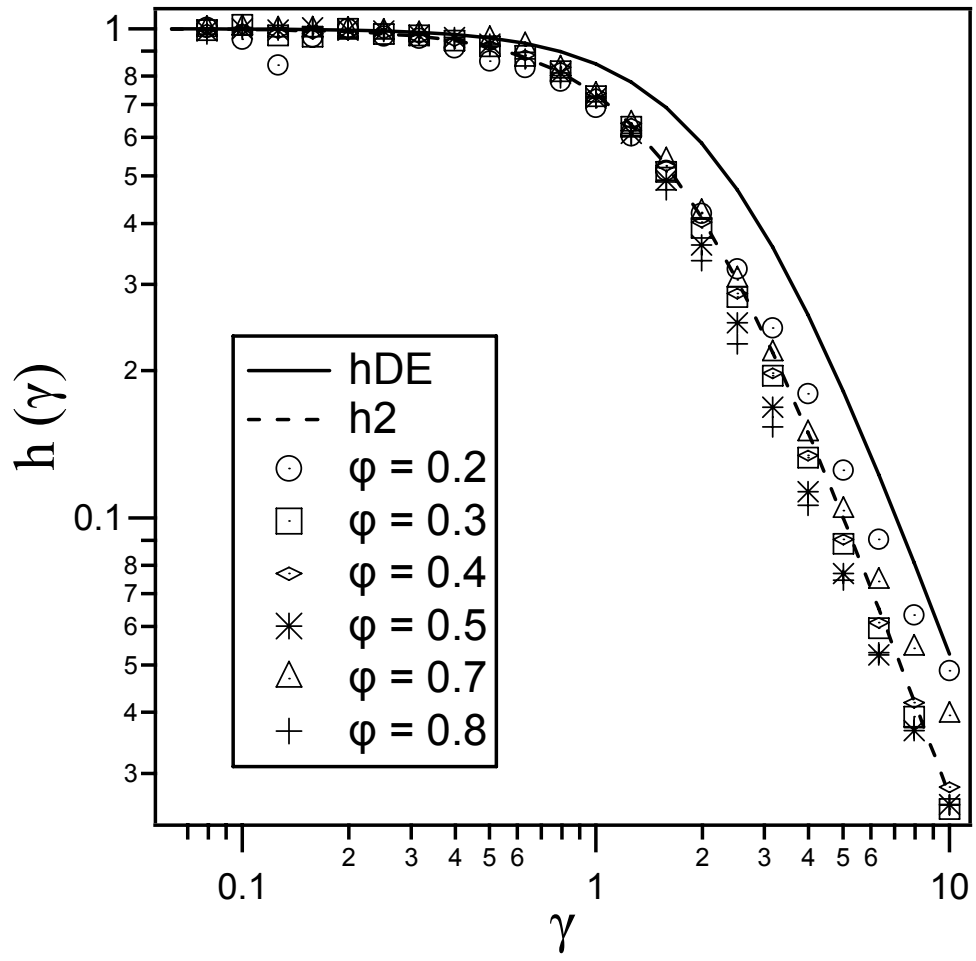

Figure 5.4: Step shear damping function for **all** PI Star (S101K) solutions; $h_{D\text{-}E}(\gamma) = (1+0.18*\gamma^2)^{-1}$ and $h2(\gamma) = (1+0.36*\gamma^2)^{-1}$

5.4.2 Results and Discussion – Unentangled Polystyrene Star Melts

All of the polystyrene stars (Table 5.2) have unentangled arms and all the stars have nearly identical master curves. The master curves (Figure 5.5) show about 8 decades of frequency, and extends from the glassy modulus ($G_g \sim 10^9$) all the way down to the terminal regime. There are two maxima in the plot of dynamic viscosity as function of frequency (Figure 5.6), which correspond to distinct relaxation times. The double maximum is only observed for the stars with the highest molecular weight (R30, R29, R28). In Figure 5.6, the shorter of the two relaxation times, which is believed to the segmental mode, is the same for all the unentangled stars. This is reasonable since we would not expect the dynamics of polymer segments to be influenced by either molecular weight or architecture. Conversely, the terminal regime relaxation time, which corresponds to the second maxima, does increase with M_n.

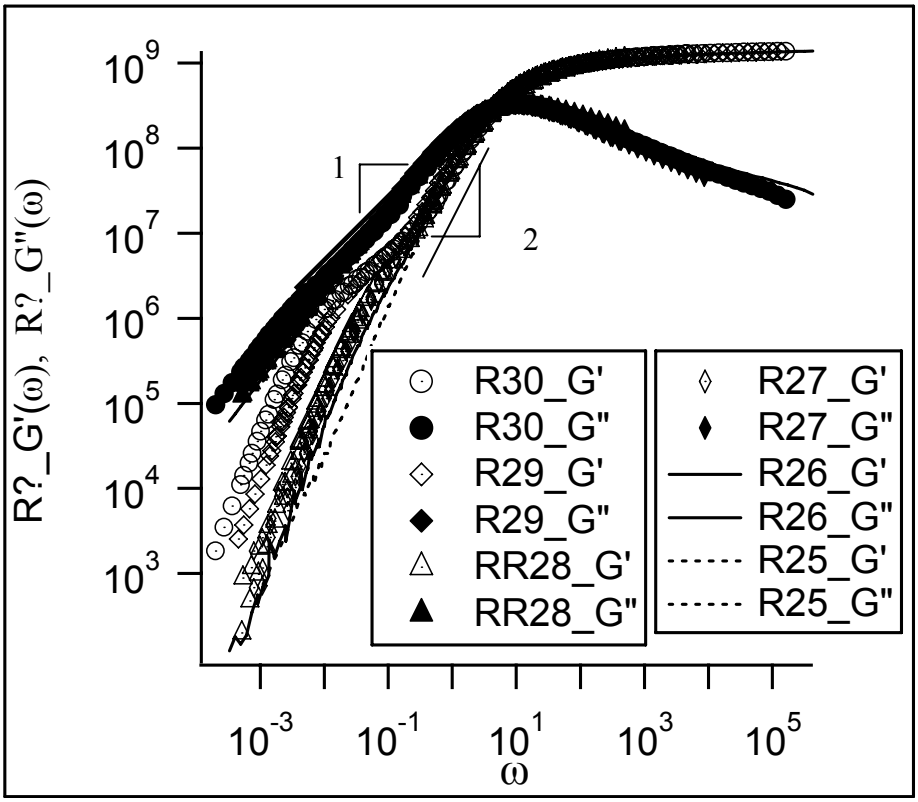

Figure 5.5: Dynamic moduli: G' (ω) and G" (ω) for unentangled 4-arm, star-branched polystyrenes

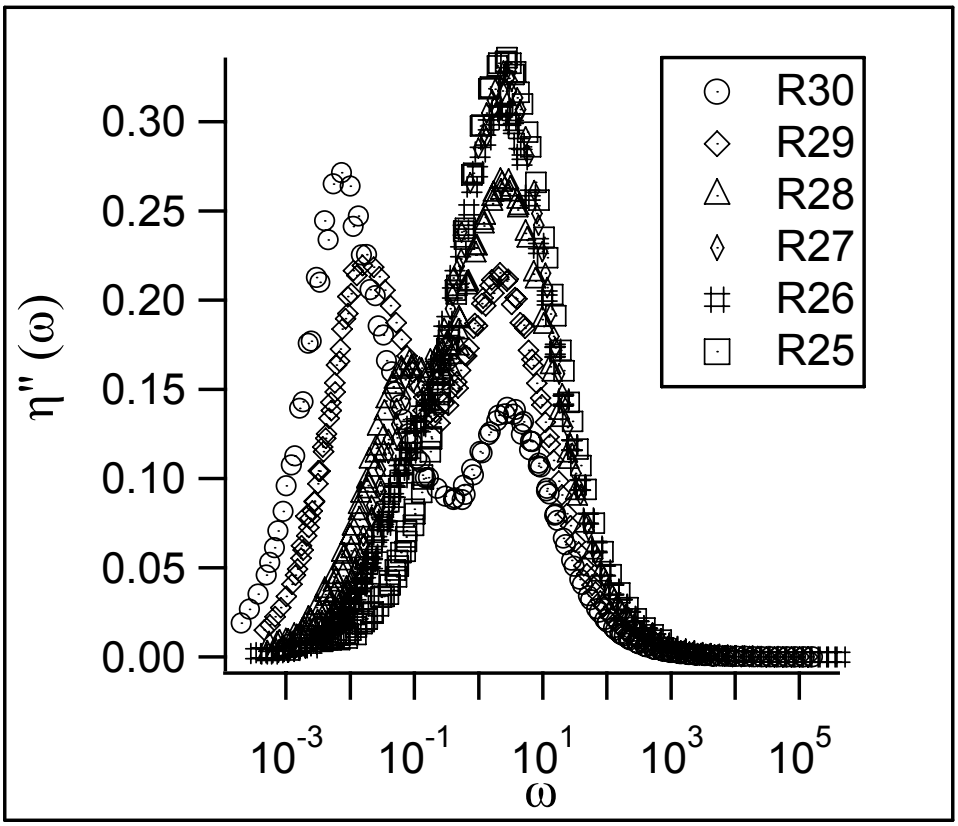

Figure 5.6: Dynamic viscosity: $\eta''(\omega)$, for unentangled 4-arm, star-branched polystyrenes measured at the respective T_g

Unentangled polymers are expected to follow the Rouse model [26] viscosity prediction: $\eta \sim N$, where N is the number of monomers in the chain. Figure 5.7 shows a directly proportional relationship between the zero shear viscosity and the polymer molecular weight. This is the expected result for polymers, which have molecular weight below the critical molecular weight for entanglement, M_c (M_c is 17-18K for PS). We also studied the short chain dependence of the glass transition temperature on molecular weight (Figure 5.8) and find that $T_g \sim 1/M_n$ as expected from:

$$T_g = T_{g,\infty} - \frac{C}{M_n} \qquad \ldots(5.1)$$

Where $C \sim 10^5$ K g mol^{-1} and $T_{g,\infty}$ is around 100ºC which is consistent with previous data [27, 28].

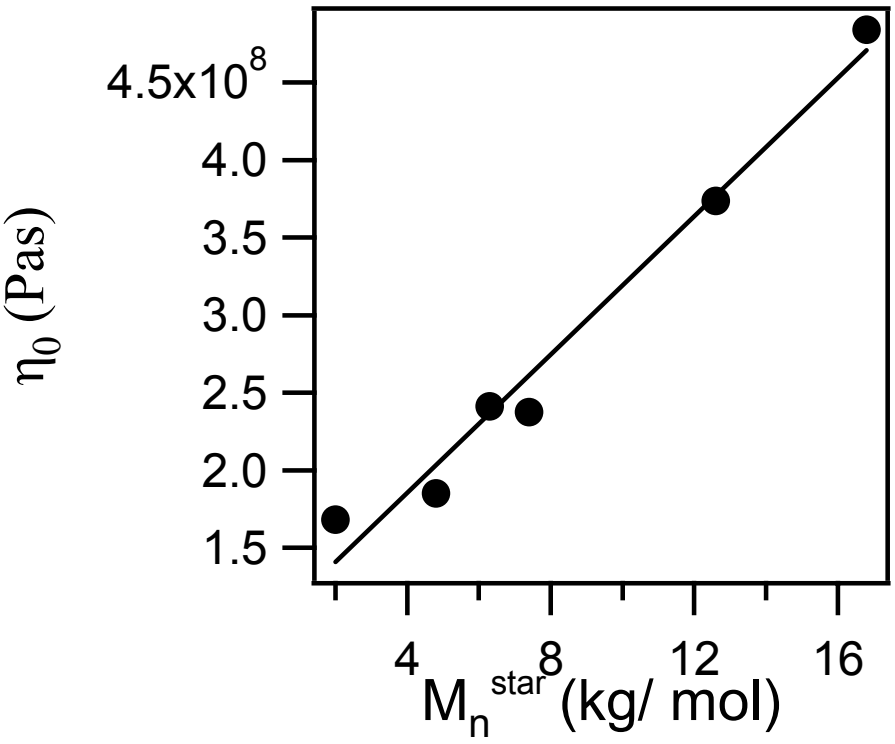

Figure 5.7: Relationship between viscosity and molecular weight for unentangled star-branched polystyrene melts.

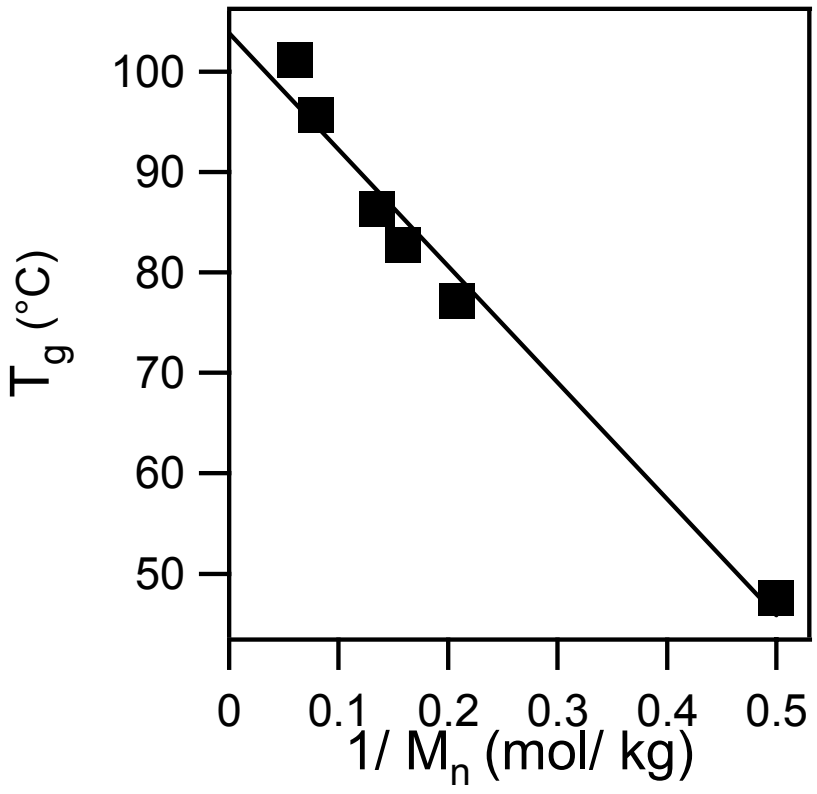

Figure 5.8: Glass transition temperature vs. inverse molecular weight for unentangled star-branched polystyrene melts

Very little is known about the nonlinear viscoelasticity of unentangled branched polymers. In step shear experiments, the relaxation of these short arm stars is very fast; in fact, the stress relaxes almost completely in less than a second (see Figures 5.9 & 5.10). Figure 5.11 shows that the damping function is either exactly the h (γ) = 1 Rouse prediction (for the shortest arm stars) or lies in-between the Rouse and D-E damping predictions (for the largest of the unentangled stars).

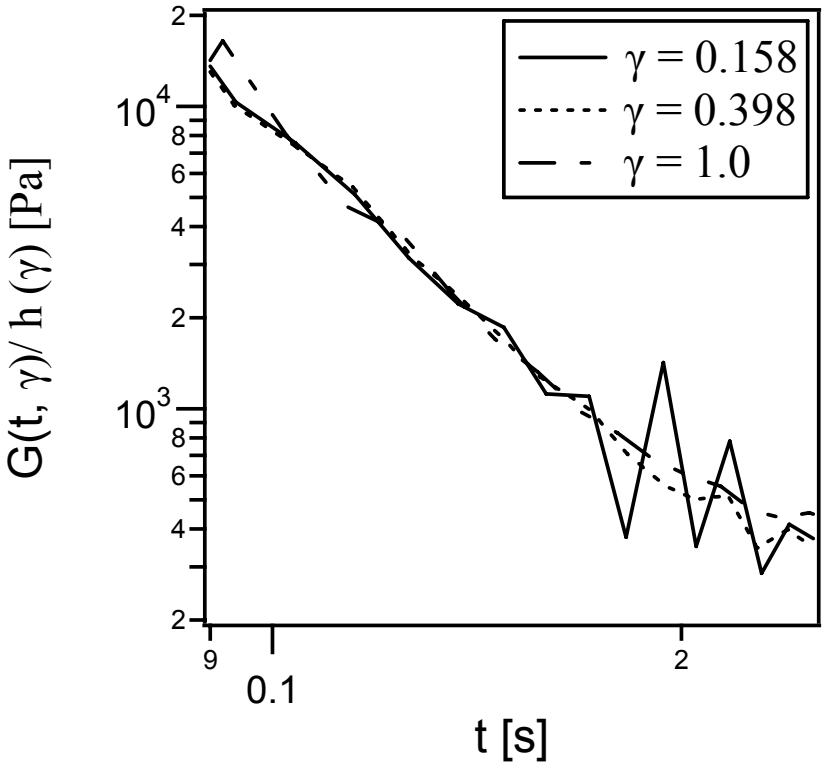

Figure 5.9: Stress relaxation of unentangled PS star: R27 (M_n^{star} = 6.3 K)

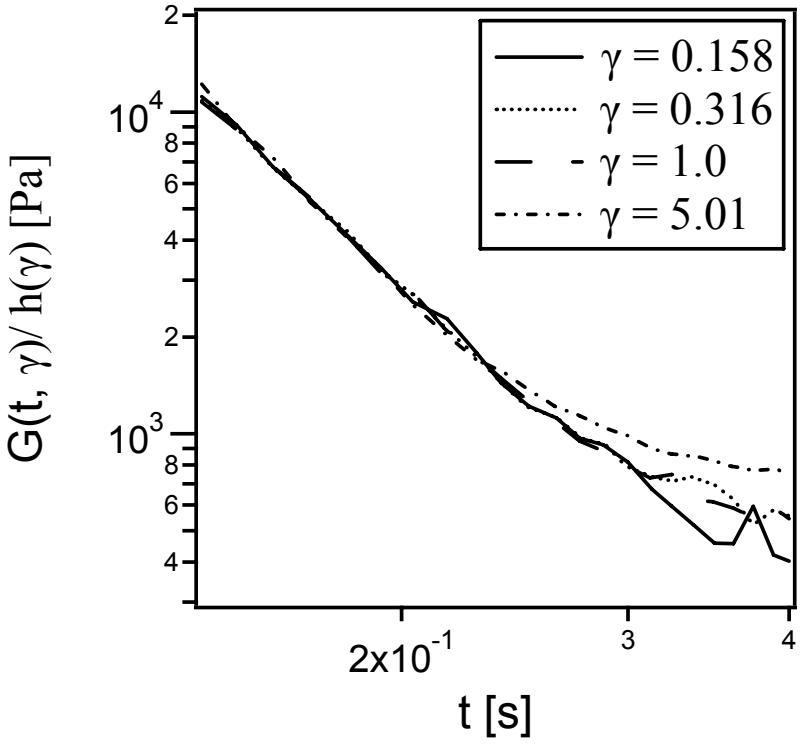

Figure 5.10: Stress relaxation of unentangled PS star: R30 (M_n^{star} = 16.8K)

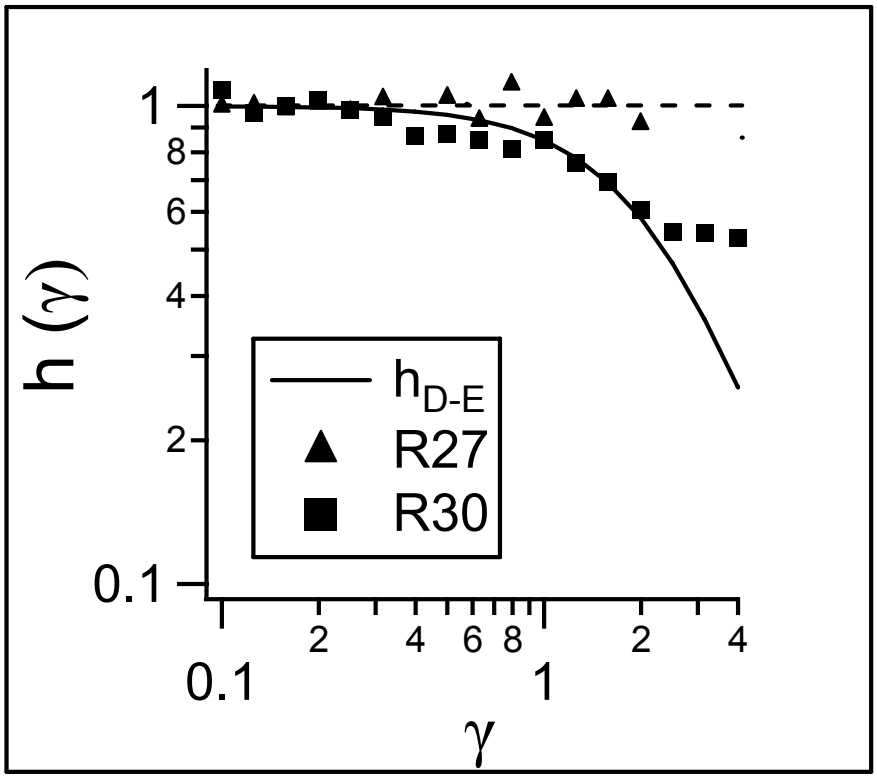

Figure 5.11: Damping function for unentangled polystyrene stars (R27 & R30)

5.5 Conclusion

Linear and nonlinear viscoelasticity of entangled star solutions and unentangled star melts is studied experimentally. As the entanglement density decreases to the unentangled state, the polymer behaves increasingly Rouse-like. LVE data for the unentangled stars detects the both glassy and terminal relaxation modes. The short-arm stars also display Rouse characteristics: $\eta \sim M_n$ and $T_g \sim 1/ M_n$. And, the measured step shear damping function of the shortest of the unentangled stars is h (γ) =1, a result which heretofore has not been measured. The entangled star solutions have their own unique (non-DE) damping function: $h2 = (1+0.36*\gamma^2)^{-1}$, which is valid for a range of entanglement densities, from scarcely to moderately entangled solutions.

REFERENCES

1) M. Doi and S. F. Edwards, *The Theory of Polymer Dynamics* (Oxford, New York, 1986).
2) C. M. Vrentas and W. W. Graessley, J. Rheol. **26**, 359 (1982).
3) F. A. Morrison and R. G. Larson, J. Polym. Sci., Polym. Phys. Ed. **30**, 943 (1992).
4) K. Osaki, Rheol. Acta **32**, 429 (1993).
5) M. T. Islam, J. Sanchez-Reyes, and L. A. Archer, J. Rheol. **45**, 61 (2001).
6) J. Sanchez-Reyes and L. A. Archer, Macromolecules **35,** 5194 (2002).
7) T. Inoue and K. Osaki, Journal of the Society of Rheology - Japan **31,** 207 (2003).
8) L. A. Archer and Juliani, Macromolecules **37**, 1076 (2004).
9) D. Vega and S. T. Milner, J. Polym. Sci., Polym. Phys. Ed. **45**, 3117 (2007).
10) H. Watanbe *et al*., Macromolecules **38,** 7404 (2005).
11) Juliani and L. A. Archer, Macromolecules **35**, 6953 (2002).
12) Van Rumbekye *et al.*, Macromolecules **40,** 1713 (2007).
13) P.G. De Gennes, J. Chem. Phys. **55**, 572 (1971).
14) S. T. Milner and T. C. B. McLeish, Macromolecules **30**, 2159 (1997).
15) R. C. Ball and T. C. B. McLeish, Macromolecules **22**, 1911 (1989).
16) J. H. Lee, L. J. Fetters and L. A. Archer, Macromolecules **38,** 3917 (2005).
17) J. H. Lee, L. J. Fetters and L. A. Archer, Macromolecules **38,** 4484 (2005).
18) A. Frischknecht *et al*., Macromolecules **35**, 4801 (2002).
19) K. Osaki et *al.*, Macromolecules **23**, 4392 (1990).
20) D. K. Bick and T. C. B. McLeish, Phys Rev Lett. **76**, 2587 (1996).

21) P. G. Santangelo *et al*., Macromolecules **32**, 1972 (1999).

22) R. Kapnistos *et al*., Rheol Acta **46**, 273 (2006).

23) J. H. Lee *et al.,* Macromolecules **39,** 6677 (2006).

24) L. A. Archer, J. Rheol. **43**, 1555 (1999).

25) M.T. Islam, J. Sanchez-Reyes, and L. A. Archer, J. Rheol. **45**, 61 (2001).

26) P. E. Rouse, J. Chem. Phys. **21**, 1272 (1953).

27) D. M. Knauss and H. A. Al-Muallem, J. Polym. Sci., Polym. Chem. **38**, 4289 (2000).

28) J. S. Lee, R. P. Quirk, and M. D. Foster, Macromolecules **38**, 5381 (2005).

APPENDIX

Nonlinear Rheology of Unentangled Linear Polystyrene Melts

A.1 Short (5-44K) Linear Polystyrenes

A study of linear and nonlinear viscoelasticity of unentangled linear polymers (Table A.1) was done. The flow behavior of these systems is thought to be best described by the Rouse model [1953].Figures A1 and A.2 show dynamic storage and loss moduli, G'(ω) and G"(ω), for the unentangled & scarcely entangled linear polystyrenes. In all cases, the reference temperature for Time Temperature Superposition (TTS) was 10 degrees higher than the Tg of the respective polymer. The superimposed master curve shows the rheological response for about 7 decades of temperature. We are only able to characterizes the terminal response with $G' \sim \omega^2$ and $G'' \sim \omega$. The graphs reveal that, for these short polymer chains, the longest relaxation time (i.e. the inverse crossover frequency) is shorter than 0.01 s.

Table A.1: Properties for Linear Polystyrene Melts

Mw (kg/mol)	**Tg (°C)**	**η_0 [Pas]**
5	91.2	9.3×10^4
8	98.3	1.39×10^5
12	101.4	2.44×10^5
13.7	101	2.38×10^5
44	108.4	2.18×10^6

- T_g measurement for all the polymers obtained is maximum in G" vs. T
- η_0 is obtained directly from the oscillatory shear data: $\eta_0 = G''/\omega$ ($\omega \rightarrow 0$) evaluated for dynamic data collected at $T_g + 20$.

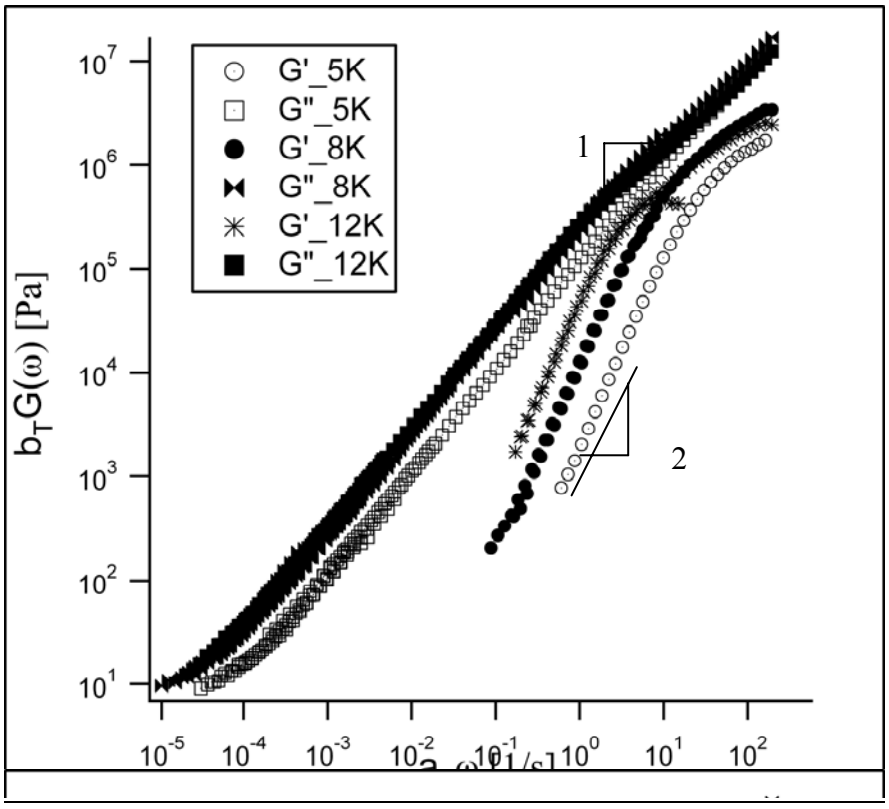

Figure A.1: Dynamic moduli, G'(ω) and G"(ω) for short linear polystyrene: 5, 8 & 12 K

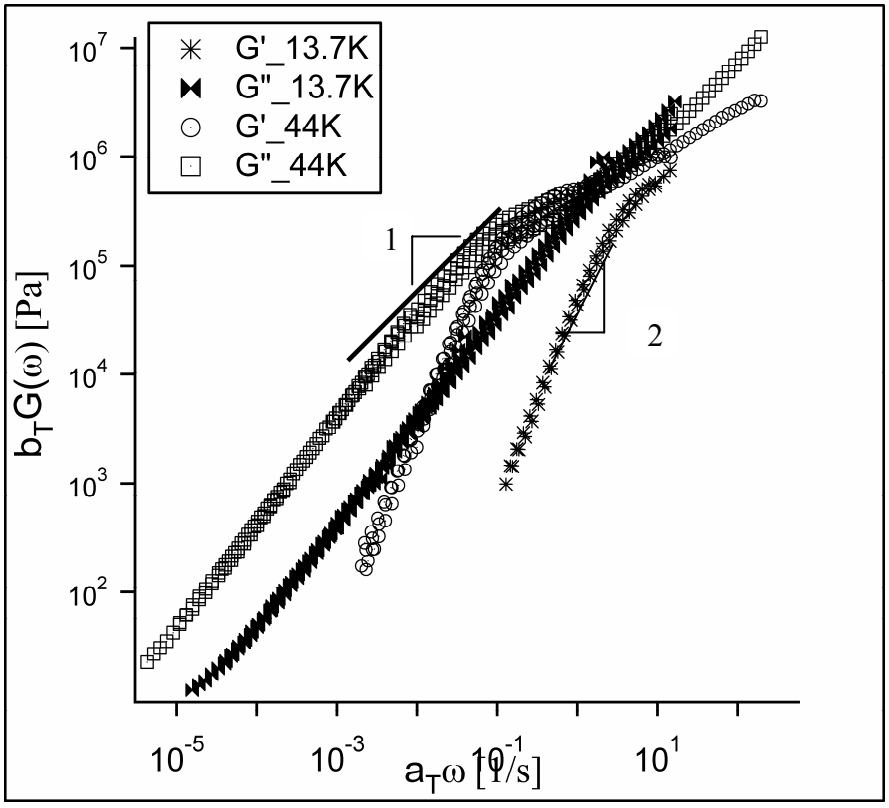

Figure A.2: Dynamic moduli, G'(ω) and G"(ω) for short linear polystyrene: 13.7 & 44 K

As in Chapter 5 we check the Rouse model viscosity prediction: $\eta \sim N$ and the short chain dependence of the glass transition temperature on molecular weight (c.f. Figures 5.7 and 5.8). As in the unentangled stars, here we measure a directly proportional relationship between the zero shear viscosity and the polymer molecular weight (Figure A.3). We find that $T_g \sim 1/ M_n$ and compare it to the stars results (Figure A.4). For both lines $C \sim 10^5$ K g mol^{-1} and $T_{g,\infty}$ is around 100ºC and is similar for both linear and stars.

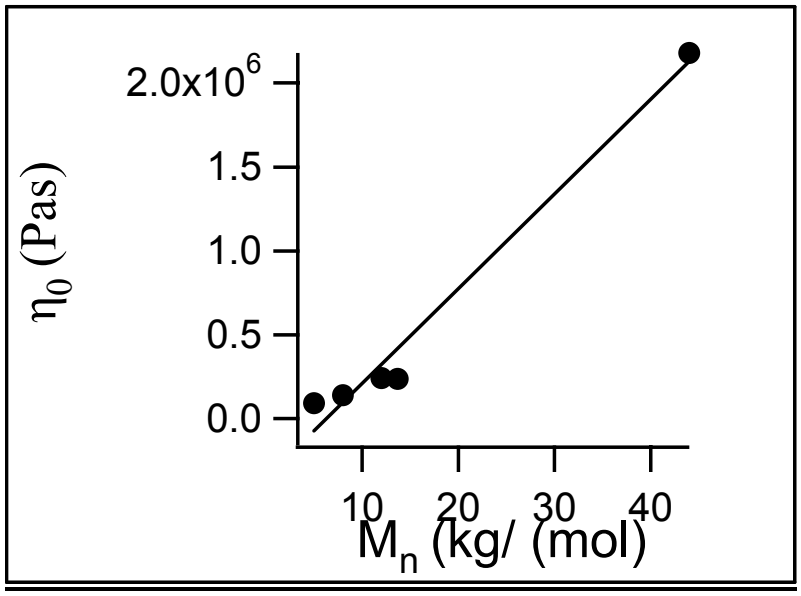

Figure A.3: Relationship between Viscosity and molecular weight for linear polystyrene

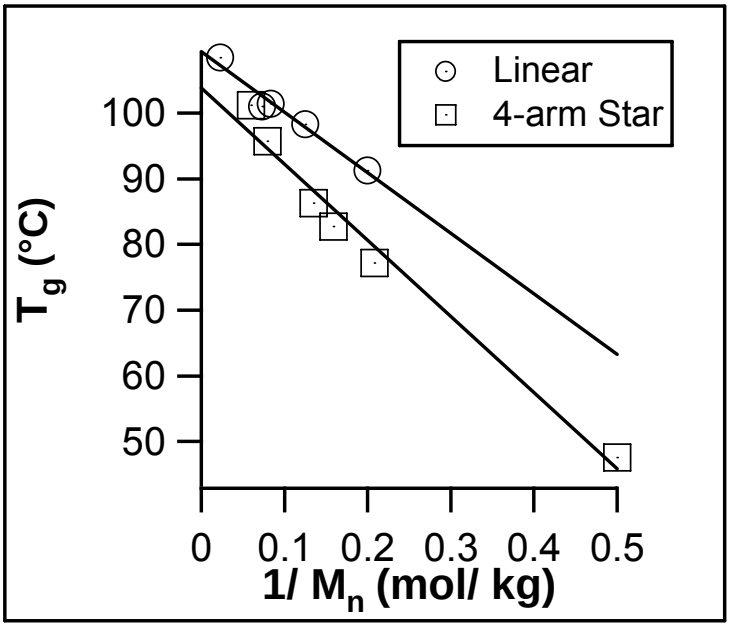

Figure A.4: Glass transition temperature vs. inverse molecular weight for unentangled linear &star Polystyrene melts

Step shear experiments (Figure A.5) were performed at a temperature of (Tg + 20) for each melt. For these unentangled polymers, there is time-strain factorability on all time scales after strain imposition. The damping function (Figure A.6) for the lowest molecular weight polymer (M_n = 5K) is close to the Rouse model prediction: h (γ) = 1. As molecular weight increases there is a transition from Type B to Type A Damping and it is surprising that for polymers with as little as 2-3 entanglements per chain, the damping function shows weak Type C behavior.

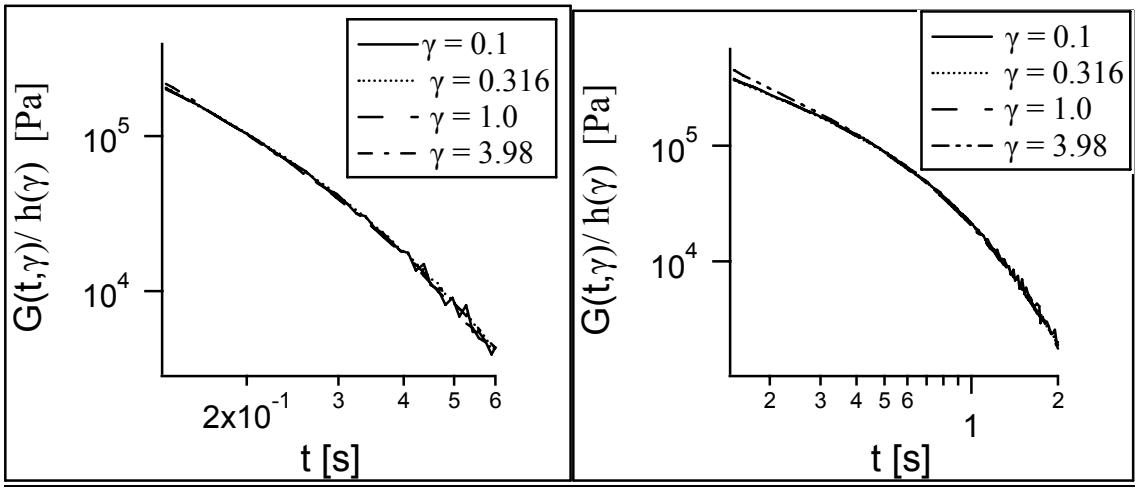

(a) – 8K (b) – 12K

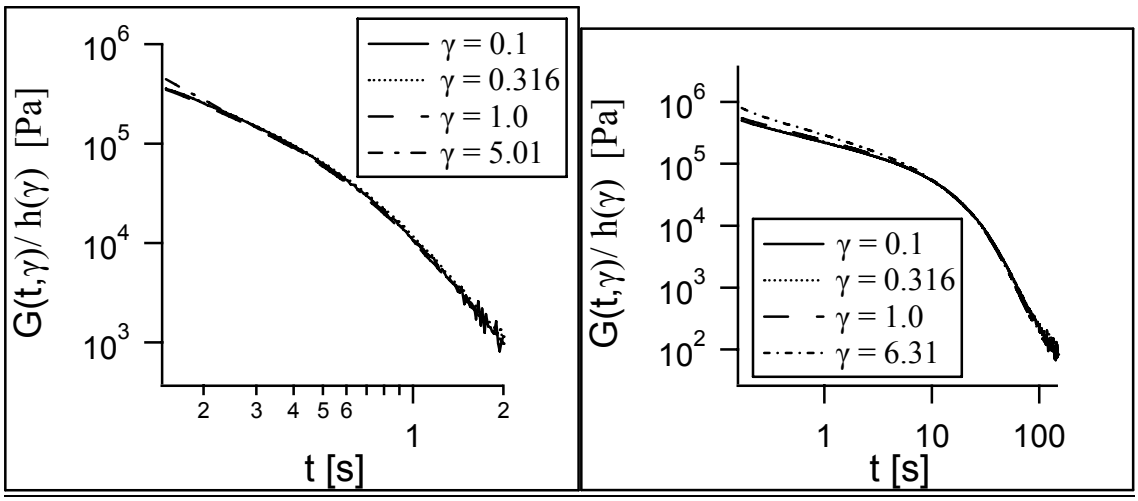

(c) – 13.7 K (d) – 44 K

Figure A.5: Shifted non-linear modulus G (t, γ) for Short Polystyrene Linear Polymers (5-44K)

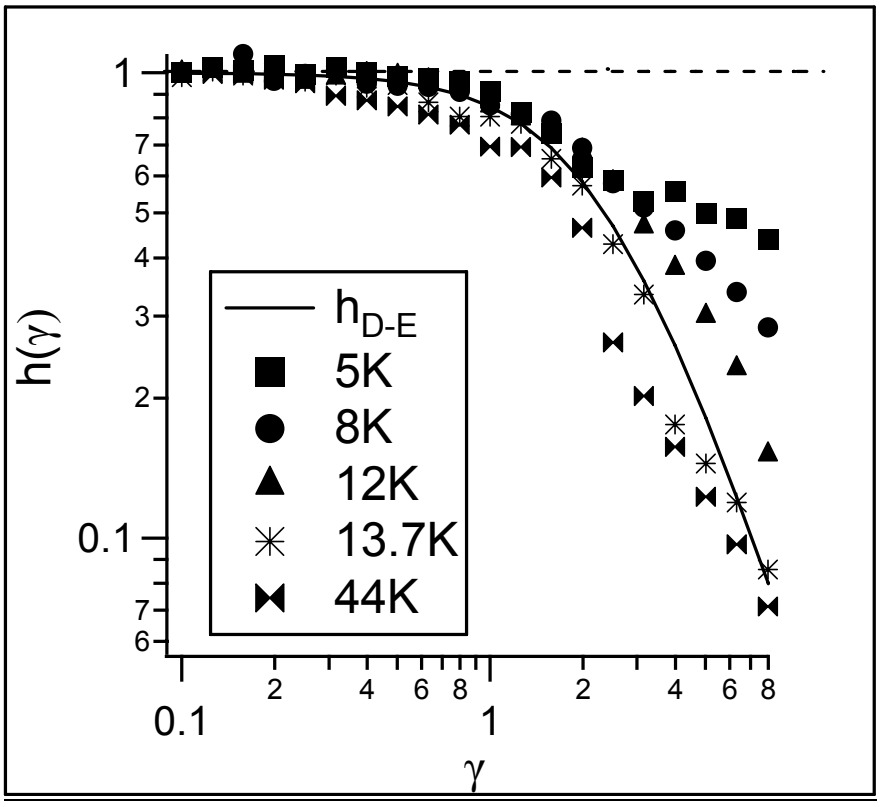

Figure A.6: Step shear damping function for **all** linear polystyrene melts $h_{D\text{-}E}(\gamma) = (1+0.18*\gamma^2)^{-1}$